A&A 462, 1103–1112 (2007)
DOI: 10.1051/0004-6361:20066365

Astronomy & Astrophysics

Pulsation in the atmosphere of the roAp star HD 24712

I. Spectroscopic observations and radial velocity measurements⋆,⋆⋆

T. Ryabchikova[1,2], M. Sachkov[2], W. W. Weiss[1], T. Kallinger[1], O. Kochukhov[3], S. Bagnulo[4], I. Ilyin[5], J. D. Landstreet[6], F. Leone[7], G. Lo Curto[3], T. Lüftinger[1], D. Lyashko[8], and A. Magazzù[9]

[1] Institut für Astronomie, Universität Wien, Türkenschanzstrasse 17, 1180 Wien, Austria
[2] Institute of Astronomy, Russian Academy of Sciences, Pyatnitskaya 48, 119017 Moscow, Russia
e-mail: ryabchik@inasan.ru
[3] Department of Astronomy and Space Physics, Uppsala University Box 515, 751 20 Uppsala, Sweden
[4] European Southern Observatory, Casilla 19001, Santiago 19, Chile
[5] Astrophysikalisches Institut Potsdam, An der Sternwarte 16, 14482 Potsdam, Germany
[6] Department of Physics and Astronomy, University of Western Ontario, London, Ontario N6A 3K7, Canada
[7] Dipartimento di Fisica ed Astronomia, Università di Catania, via S. Sofia 78, 95123 Catania, Italy
[8] Tavrian National University, Simferopol, Ukraine
[9] INAF – Telescopio Nazionale Galileo, PO Box 565, 38700 Santa Cruz de La Palma, Spain

Received 8 September 2006 / Accepted 8 November 2006

ABSTRACT

Aims. We have investigated the structure of the pulsating atmosphere of one of the best studied rapidly oscillating Ap stars, HD 24712.
Methods. For this purpose we analyzed spectra collected during 2001–2004. An extensive data set was obtained in 2004 simultaneously with the photometry of the Canadian MOST mini-satellite. This allows us to connect directly atmospheric dynamics observed as radial velocity variations with light variations seen in photometry.
Results. We directly derived for the first time and for different chemical elements, respectively ions, phase shifts between photometric and radial velocity pulsation maxima indicating, as we suggest, different line formation depths in the atmosphere. This allowed us to estimate for the first time the propagation velocity of a pulsation wave in the outer stellar atmosphere of a roAp star to be slightly lower than the sound speed. We confirm large pulsation amplitudes (150–400 m s^{-1}) for REE lines and the Hα core, while spectral lines of the other elements (Mg, Si, Ca, and Fe-peak elements) have nearly constant velocities. We did not find different pulsation amplitudes and phases for the lines of rare-earth elements before and after the Balmer jump, which supports the hypothesis of REE concentration in the upper atmosphere above the hydrogen line-forming layers. We also discuss radial velocity amplitudes and phases measured for individual spectral lines as tools for a 3D tomography of the atmosphere of HD 24712.

Key words. stars: atmospheres – stars: chemically peculiar – stars: individual: HD 24712 – stars: magnetic fields – stars: oscillations

1. Introduction

About 10% to 20% of upper main sequence stars are characterized by remarkably rich line spectra, often containing numerous unidentified features. Compared to the solar case, overabundances of up to a few dex are often inferred for some iron peak and rare earth elements, whereas some other chemical elements are found to be underabundant (Ryabchikova et al. 2004). Some of these *Chemically Peculiar* (CP) stars also exhibit organized magnetic fields with a typical strength of a few kG. The specific chemical peculiarities observed are believed to result from the influence of the magnetic field on the diffusing ions, possibly in combination with the influence of a weak, magnetically directed wind (e.g., Babel 1992).

More than 30 cool CP stars exhibit an additional peculiarity, which is high-overtone, low-degree, non-radial *p*-mode pulsation with periods in the range of 6–21 min, with their observed pulsation amplitudes modulated according to the visible magnetic field structure. These so-called rapidly oscillating peculiar A to F-type (roAp) stars are key objects for asteroseismology, which presently is the most powerful tool for testing theories of stellar structure and evolution. Spectroscopic and photometric techniques provide information on the boundary zone relevant for any pulsation model, and open access to different modes and hence atmospheric layers. An observed phase lag between luminosity and radial velocity variations is an important parameter for a first step towards modeling the stellar structure. The dependency of radial velocity amplitudes as a function of optical depths lead to a 3D tomography of the stellar atmosphere.

The best studied multi-periodic roAp star presently is HD 24712, which makes this star a cornerstone for stellar seismology, even beyond the class of CP stars. It was discovered to be a pulsator by Kurtz (1982) with periods around 6 min, and Matthews et al. (1988) found synchronized radial velocity

⋆ Based on observations collected at the Canada-France-Hawaii Telescope (CFHT), at the Nordic Optical Telescope (NOT), at the European Southern Observatory, Paranal, Chile, (DDT-274.D-5011), at the Telescopio Nazionale Galileo (TNG), and from MOST, a Canadian Space Agency mission operated jointly by Dynacon, Inc., the University of Toronto Institute of Aerospace Studies, and the University of British Columbia, with assistance from the University of Vienna.
⋆⋆ Tables 4, 5 and Fig. 9 are only available in electronic form at http://www.aanda.org

variations. Photometry with the Whole Earth Telescope (WET, Kurtz et al. 2002) revealed a "missing" mode, suggesting that *p*-mode pulsation are strongly affected by the global stellar magnetic field, an aspect which was investigated in detail by Cunha et al. (2003) and by Cunha (2006).

These characteristics made HD 24712 a very strong candidate for contemporaneous spectroscopic observations with large ground based equipment suited to obtain high time resolution, high spectral resolution, and high signal-to-noise ratio spectra simultaneously with high precision photometric observations with MOST, the Canadian photometric space telescope (Walker et al. 2003). The MOST instrument is a 15-cm Maksutov type optical telescope feeding twin CCD detectors through a broadband filter (350–700 nm). The equipment was designed to obtain rapid photometry of bright stars for up to 2 months and with a nearly 100% duty cycle. Despite its low mass of only 54 kg (and hence little inertia) it is able to perform optical photometry of point sources due to a pointing accuracy of better than $\pm 1''$ rms (Walker et al. 2003).

MOST observed HD 24712 continuously from Nov. 5, to Dec. 4, 2004, and a parallel ground based observing campaign was organized which yielded the spectroscopic time series listed in the last five lines of Table 1. While the main photometric results will be published elsewhere, we focus here on the spectroscopic analysis and are using MOST data primarily for a direct comparison of the data taken simultaneously in space and from ground.

2. Observations and spectra reduction

The observations of HD 24712 were collected during 13 nights: Oct. 2–4, 2001; Sep. 23–26, 2002; Nov. 6, 2003; Nov. 11–13, 15, and Dec. 2, 2004. The journal of observations is given in Table 1, which lists set numbers, civil dates, heliocentric Julian dates of the start of the observing sequence, spectral range, run duration in hours, and the number of spectra that were obtained in each night. The chosen exposure times are a compromise between the requirement to integrate the spectrum only over a small fraction of the pulsation period, and the need to have a reasonable signal-to-noise (S/N) ratio for each spectrum. The seventh column gives the rotation phases for the mean time of each data set according to the ephemeris given by Ryabchikova et al. (2005b):

$$\mathrm{HJD}(\langle B_z\rangle_{\max}) = 2\,453\,235.18(40) + 12.45877(16)\,\mathrm{d}.$$

Heliocentric Julian dates are given for the centre of exposures. The heliocentric corrections were applied to spectroscopic observations and to MOST photometry in the same way.

2.1. Time-series of single-order spectra

- *GECKO*: the observations of 2001 and 2002 were obtained with the single-order $f/4$ GECKO Coudé spectrograph and the EEV1-CCD at the 3.6-m Canada-France-Hawaii telescope. The spectra have a resolving power of about 115 000, determined from the widths of a number of ThAr comparison lines. The exposure time was 60 s, dead time was 44 s, and the achieved S/N in the continuum was about 100. These observations covered 7 spectral regions centered approximately at 4860, 5300, 5855, 6160, 6600, 6675, and 7780 Å, containing the most interesting spectral lines of singly and doubly-ionized rare earth elements (REE), Hα, Hβ, O I, Fe I, Ca I, and Ba II.

The spectra were reduced using standard IRAF tasks. Each stellar, flat and calibration frame had a mean bias subtracted and was then cleaned of cosmic ray hits and collapsed to one dimension. The spectra were divided by a mean flat-field, extracted in the same way, and the continuum was fitted with a three-segment cubic spline, using the same rejection parameters for all spectra so that the continuum fit is as uniform as possible.

The wavelength scale was established using about 40 lines of a ThAr emission lamp, resulting in an rms scatter of about 3×10^{-4} Å. The wavelength scale was linearly interpolated between ThAr lamp spectra taken before and after the stellar series, but the spectra were not sampled to a linear wavelength spacing.

2.2. Time-series of échelle spectra

- *SOFIN*: the observations from Nov. 6, 2003, were carried out with the SOFIN high resolution échelle spectrograph at the 2.56 m Nordic Optical Telescope (NOT), La Palma, Spain. Each spectrum had an integration time of 50 s with a readout time of 55 s, giving a time-resolution of 105 s. The typical S/N ratio is about 80 and the resolving power ≈80 000. These échelle spectra cover the region from 5000 to 6800 Å. The échelle images were reduced with the Advanced Acquisition, Archiving, and Analysis (4A) package written in C (Ilyin 2000).

The standard reduction sequence includes bias subtraction from the CCD overscan, photon noise estimation for the pixel variances, correction for the CCD fixed pattern noise using a master flat field (a sum of 100 exposures), subtraction of the scattered light determined from a 2D spline fit to the inter-order gaps. The spectral order position is found from the flat field image and subsequently adjusted for each échelle science frame. This step is followed by a weighted extraction of spectral orders with elimination of cosmic spikes based on a linear regression. The shape of the spectra and fringes in the red part of the CCD are corrected with a flat field spectrum smoothed with a spline fit. The wavelength calibration is based on about 1300 ThAr spectral lines collected from two successive images, using a 2D fit to them, taking also the time of exposures for calibration and science frames into account. A zero point correction had to be applied which resulted in a final RV error of about 25 m s^{-1} at the image center.

- *HARPS* and *UVES*: the 2004 spectroscopic observation were carried out with HARPS (High Accuracy Radial velocity Planet Searcher) spectrometer at the 3.6-m telescope at ESO, La Silla. 92 spectra with 60 s exposure time, $S/N = 120$, and 120 000 resolving power were taken during November 10/11, 2004, simultaneously with MOST. Because of the unique coincidence with the space photometry, Director's Discretionary Time (274.D-5011) was granted for November 11/12 and 12/13 with the UVES spectrograph at the 8.2-m telescope, UT2 (Kueyen), of the VLT on Paranal, Chile, (92 and 73 spectra, 50 s exposure time, $S/N = 300$, with a resolving power of about 80 000).

All spectra were reduced and normalized to the continuum level with a routine specially developed by one of us (DL) for a fast reduction of time-series observations. It is a component of the spectral reduction package STAR XP, a special modification of the Vienna automatic pipeline for échelle spectra processing (Tsymbal et al. 2003). All bias and flat field images were median averaged before calibration. The scattered light was subtracted by using a 2D background approximation. For cleaning of cosmic rays we used a new algorithm which compares the direct and reversed spectral profiles. To determine the spectrum order boundaries, the code uses a special template for each order position in each row across the dispersion axis. The shift of the row spectra relative to the template is derived by a cross-correlation

Table 1. Journal of time-resolved spectroscopy of HD 24712. Listed are, among others, the duration of a continuous set of observations (Run, in hours) in a given night and the number of individual spectra taken during such a run, and the typical S/N ratio for the continuum.

Set No.	Civil date (UT)	Start HJD (2 450 000+)	Spectral range (Å)	Run (h)	No. of spectra	Exposure time (s)	Overhead time (s)	Typical S/N	Rot. phase	Instr.
1	2001.10.02	2 185.15654	6106–6189	3.77	123	60	42	100	0.71	GECKO
2	2001.10.03	2 186.15303	6106–6189	4.60	162	60	41	100	0.79	GECKO
3	2001.10.04	2 187.15230	6620–6730	4.77	163	60	42	100	0.87	GECKO
4	2002.09.23	2 541.08000	5822–5887	2.44	82	60	44	100	0.28	GECKO
5	2002.09.24	2 541.16417	6543–6658	1.43	49	60	44	100	0.29	GECKO
6	2002.09.24	2 542.02444	5822–5887	2.03	66	60	44	100	0.36	GECKO
7	2002.09.25	2 542.11958	5284–5344	1.96	66	60	44	100	0.37	GECKO
8	2002.09.25	2 543.05228	5822–5887	1.89	65	60	44	100	0.44	GECKO
9	2002.09.26	2 543.14946	6105–6195	1.84	64	60	44	100	0.45	GECKO
10	2002.09.26	2 544.14997	5822–5887	3.81	127	60	44	100	0.53	GECKO
11	2003.11.06	2 949.69312	4540–9952	1.58	53	50	55	80	0.08	SOFIN
12	2004.11.11	3 320.78693	3850–6730	2.31	92	60	30	120	0.87	HARPS
13	2004.11.12	3 321.74421	3400–6720	2.09	92	50	30	300	0.94	UVES
14	2004.11.13	3 322.77598	3400–6720	1.73	73	50	30	300	0.03	UVES
15	2004.11.15	3 324.60032	4575–7872	1.07	35	60	52	120	0.18	SARG
16	2004.12.02	3 341.66789	4575–7872	1.13	33	60	52	120	0.55	SARG

technique. Wavelength calibration was done by the usual 2D fit. The accuracy of this procedure is $\approx 20\,\mathrm{m\,s^{-1}}$. The final step of continuum normalization was done by transforming of the flat field blaze function to the response function in each order.

- *SARG*: during MOST observations of HD 24712, additional spectra were obtained in Nov. 14/15, 2004, (35 spectra), and on Dec. 01/02, 2004, (33 spectra), with the high resolution spectrograph (SARG) at the 3.55-m *Telescopio Nazionale Galileo* (TNG) at the Observatorio del Roque de los Muchachos (La Palma, Spain). The spectra were reduced using standard ESO-MIDAS software with the same main steps as described above. The spectra cover the range of 4570–7900 Å, have a resolving power of about 57 000 and a S/N ratio of approximately 120. The time resolution was 129 s (60 s for exposure and 69 s for read out).

2.3. Polarimetry with SOFIN

The spectropolarimetric observations of HD 24712 were carried out between Oct. 29, and Nov. 18, 2003, with the high resolution échelle spectrograph, SOFIN, attached to the Cassegrain focus of NOT. The spectrograph is equipped with three different cameras offering three different resolving powers. To obtain observations in the polarimetric mode, the second camera with a resolving power of ≈80 000 was used. Between 4000–7000 Å seven spectral orders, each covering about 40 to 50 Å were used for the magnetic field analysis.

The circularly polarized spectra were obtained with a Stokesmeter, consisting of a fixed achromatic quarter-wave plate, a beam splitter made of a calcite plate, and an achromatic rotating quarter-wave plate, whose position is controlled by a stepping motor. To obtain accurate circular polarization measurements, usually a sequence of four exposures is obtained. Each of the beams is exposed twice, with the quarter-wave plate rotated by 90° after the first and before the last exposure. Such a sequence reduces instrumental effects to a minimum, because in the images taken with the quarter-wave plate rotated by 90°, instrumental signatures change sign and cancel when averaging the two exposures.

Data reduction was performed with the aforementioned 4A software package including all standard procedures, such as bias subtraction, flat field correction, subtraction of the scattered light, weighted extraction of the orders, and bad pixel (cosmic ray) corrections. ThAr exposures obtained before and after each observing night were used to perform wavelength calibration and to test for possible spurious instrumental polarization, caused e.g. by bending of the spectrograph which is directly mounted on the telescope, different positions of the star on the slit, or temporal variations of the seeing. S/N ratios for the observed spectra are typically 200–300. Rotation phases of HD 24712 (see Table 2) were calculated according to the ephemeris and rotation period derived by Ryabchikova et al. (2005b).

Table 2. Journal of spectropolarimetric observations of HD 24712. The longitudinal field $\langle B_z \rangle$ was estimated using ten Nd II and Nd III lines (3rd column), and seven Cr I, Cr II, and Fe I lines (4th column).

HJD (2 450 000+)	Rotation phase	$\langle B_z \rangle$ (G) Nd II, Nd III	Cr I, Cr II, Fe I
2 941.6516	0.44	598 ± 165	87 ± 68
2 943.6341	0.60	909 ± 154	240 ± 132
2 945.5758	0.76	1109 ± 105	535 ± 145
2 946.5973	0.84	1090 ± 144	729 ± 180
2 947.6067	0.92	1182 ± 100	1098 ± 98
2 948.6514	0.00	1132 ± 98	1064 ± 130
2 952.6267	0.32	835 ± 174	258 ± 79
2 953.6572	0.40	629 ± 129	155 ± 86
2 954.6316	0.48	720 ± 192	165 ± 155
2 955.6350	0.56	830 ± 187	137 ± 107
2 956.5954	0.64	1062 ± 178	260 ± 174
2 957.5958	0.72	1159 ± 164	483 ± 158
2 961.6160	0.04	1168 ± 100	1048 ± 152

3. Radial velocities and magnetic field strength

For radial velocity (RV) measurements we carefully chose unblended or minimally blended lines in the 3300–6800 Å spectral region. Between 3900 and 4400 Å the cores of the strong (resonance) lines of Ca, Fe and Sr were measured. Our choice was based on synthetic spectrum calculations over the whole spectral region of 3300–6800 Å, made with the spectral

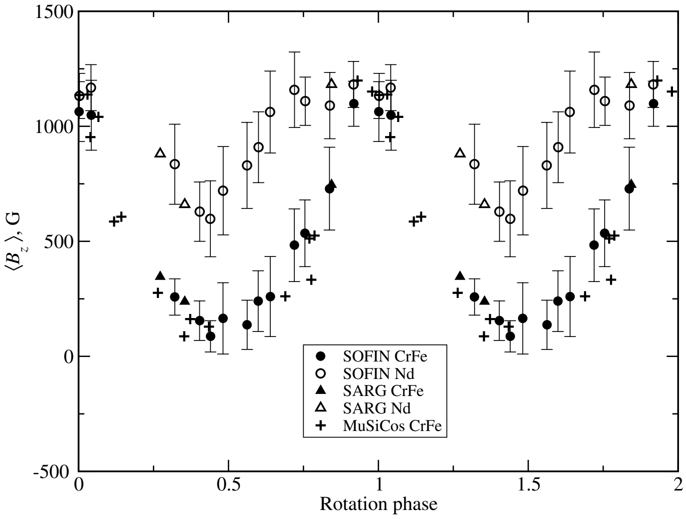

Fig. 1. Longitudinal magnetic field variations in HD 24712. Open (Nd lines) and filled (Cr-Fe lines) circles are the observations presented in this paper, open and filled triangles are magnetic measurements from Leone & Catanzaro (2004), and crosses represent data taken from Ryabchikova et al. (2005b).

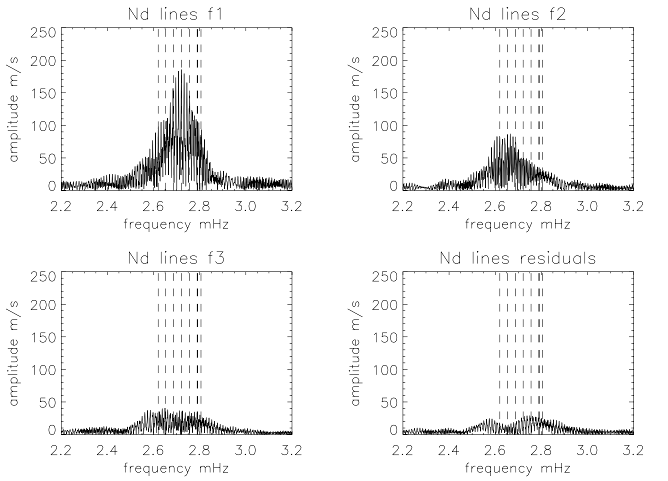

Fig. 2. Amplitude spectra of the Nd III spectral lines of the 2004 observations. The *top left panel* shows the DFT of the original RV data; the *top right panel* represents the DFT after prewhitening with the highest amplitude frequency; the *other panels* show the next prewhitening steps. Dashed lines indicate photometric frequencies according to Kurtz et al. (2005).

synthesis code SYNTH3 written by Kochukhov, and using the atmospheric parameters and abundances from Ryabchikova et al. (1997). Atomic parameters of spectral lines for the synthesis were extracted from the Vienna Atomic Line Database, VALD (Kupka et al. 1999), and from the Database for Rare Earths at Mons University, DREAM (Biémont et al. 1999), which is also accessible via the VALD extraction procedures. For the Nd III identification additional atomic data from Crosswhite (1976), Aldenius (2001) and Ryabchikova et al. (2006) were used.

The radial velocities were measured with a center-of-gravity technique and attention was payed to the stability of the spectrographs. HARPS time-resolved spectra provide stable results with a mean rms dispersion of $20\,\mathrm{m\,s^{-1}}$ per individual non-pulsating line, while a quasi-linear, long-term drift was found in both nights of the observations with UVES. These drifts were approximated with a smooth spline function based on the average measurements of a few unblended non-pulsating Fe I lines. This quasi-linear drift was then subtracted from the RV measurements of all other spectral lines. It should be emphasized that the instrumental variation of the spectrograph's zero point occurs on a much longer time scale than the stellar *p*-mode variability, and therefore does not affect the pulsation analysis presented here.

Radial velocities of more than 500 unblended spectral lines were measured in the spectral region from 3900 to 6800 Å, and additional 80 lines were measured in the region blueward the Balmer jump (BJ). A complete list of measured lines (but not all individual measurements) together with their identification is given in Table 4 (Online material). The purpose of this table is to provide line identifications and to indicate pulsating and non-pulsating lines.

The longitudinal magnetic field was measured as the first moment of the observed Stokes *V* parameter for a set of chosen spectral lines. We have performed separate measurements of the iron-peak elements (Cr and Fe) and of the REEs (Nd and Tb). The results and error estimates are given in Table 2 and are illustrated in Fig. 1. For a comparison, $\langle B_z \rangle$ data from Ryabchikova et al. (2005b – MuSiCoS) and from Leone & Catanzaro (2004 – SARG) are also included in this figure.

We found that some spectral lines with large Landé factors are partially split in non-polarized spectra. In particular one line, Cr I 5247.56 Å, is a pure triplet with $g_{\mathrm{eff}} = 2.51$, and another line, Fe II 6432.48 Å, is a pseudo-doublet with $g_{\mathrm{eff}} = 1.82$. Using these lines we estimated the magnetic modulus $\langle B \rangle$ at phases 0.867, 0.944 (close to the magnetic maximum) and at phase 0.42 (near the magnetic minimum). For the latter, a UVES spectrum of HD 24712 was extracted from the ESO archive. $\langle B \rangle$ estimates were made by fitting calculated synthetic line profiles to the observed spectra. Magnetic synthetic calculations were carried out with SYNTHMAG (Kochukhov 2006), which represents an improved version of the program described by Piskunov (1999). $\langle B \rangle$ varies between 3100–3300 G at $\langle B_z \rangle_{\max}$ and 2500 G at $\langle B_z \rangle_{\min}$ according to our estimates.

4. Frequency analysis

Although RV variations in the REE lines due to pulsation are very distinctive and the relative accuracy of individual spectroscopic data is higher than for photometry, it proved to be difficult to study in detail the frequencies of multiperiodic roAp stars by spectroscopy, because a large telescope is needed during an extended period of time. For a reliable frequency analysis it is necessary to observe continuously during weeks with a minimum of gaps. This is possible either with dedicated satellites, as is MOST for photometry, or with multisite ground based campaigns, such as WET (Kurtz et al. 2005). Although our spectroscopic monitoring does not allow for a detailed frequency analysis, we performed nevertheless such an analysis to confirm the consistency of the main frequencies in the spectroscopy obtained simultaneously with the MOST photometry.

Our Fourier analysis of the RV data of selected lines – Pr III 5284, 5300 Å, Nd III 5203, 5294, 5845, 5851, 5987, 6145 Å and Tb III 5505 Å – was based on a discrete Fourier transform (DFT) and stepwise prewhitening with a sine fit to the highest amplitudes (see Fig. 2). In this analysis we used all spectra obtained simultaneously with MOST during four nights around the magnetic maximum (sets 12 to 15). The duty cycle for this combined 4-night data set is poor (about 8%), but knowing from MOST photometry which alias to avoid, we found the 3 highest amplitude periods in our spectroscopy to be 6.125 min, 6.282 min, and 6.202 min. These values agree well with contemporaneous MOST photometry, as is illustrated in Fig. 3 for one of the pulsating lines (Pr III 5300 Å). These frequencies correspond to ν_4, ν_2, and ν_3 in Kurtz et al. (2005). The frequency analysis performed for the 2001 Nd III data gives two main frequencies ν_4 and ν_2 (identification according to Kurtz et al., op. cit.) with similar amplitudes as in 2004 (see Fig. 9 in Online Material). This figure illustrates (as does Fig. 2) the possibility to identify pulsation frequencies, amplitudes and phases even in short spectroscopic runs distributed over several nights – what results in a very poor duty cycle – provided one can avoiding aliases thanks to MOST and WET photometry.

The short observing run in 2003 does not allow us to resolve frequencies. Only one frequency close to ν_3 was derived.

Different authors prefer to characterize periodic signal either with periods or with frequencies. For convenience of the reader we mention here the conversion: period in minutes transforms to a frequency in mHz via $\nu(\mathrm{mHz}) = 16.6667/P(\mathrm{min})$.

5. Phase relations between photometry and spectroscopy

Our time-resolved observations in 2004 were carried out simultaneously with the Canadian micro–satellite MOST which monitored HD 24712 from 2004 November 6, to December 5. This provides us with the opportunity to derive directly the phase lag between photometry and spectroscopy.

This was attempted already earlier by Matthews et al. (1988) despite a rather poor S/N ratio (≈20) of their individual spectra. But the large number of spectra (≈600) allowed the authors to derive an average RV curve and to find a coincidence of RV maxima with δB minima, which corresponds to a phase lag of about 0.5, where we define a phase lag as a phase difference between the maxima of both, photometric and RV variations. They found the photometric maximum to occur typically *after* the RV maximum, which we confirm with our data.

The high S/N and spectral resolution of the present observations resulted in more precise values for phase lags, and in particular it allowed us to determine this quantity for individual spectral lines. In order to minimize the influence of the higher point-to-point scatter of the photometric data with respect to the spectroscopic observations, we computed an artificial time-series data set based on the 3 dominant frequencies and their amplitudes and phases (ν_2, ν_3 and ν_4) which were derived from the complete set of MOST observations. Next, this artificial time-series was cross-correlated with the RV observations of the individual spectral lines. The time interval for the cross correlation ranges from plus to minus 6.125 min, the latter corresponds to the period with the largest amplitude (ν_4). The time step was 1 s. The best correlation gives the time lag between photometry and spectroscopy expressed in seconds.

The time lags obtained with artificial time-series data generated with the 3 dominant frequencies differ only by ∼2 s from those obtained with a full set of frequencies which is about an order of magnitude less than the accuracy of the used correlation technique. The remaining frequencies in the full MOST frequency solution with very low amplitudes obviously do not affect the time lag determination.

In Fig. 3 we illustrate the excellent agreement between the RV variations of the Pr III spectral line and the photometric observations, shifted by about –197 s, which corresponds to a phase lag of –0.54, using the main photometric pulsation frequency. Both observations are normalized and scaled for better visibility.

The result of the cross-correlation procedure is given in Table 3. The brightness maximum occurs for all lines after the RV maximum, but the phase lag itself depends strongly on the individual line. It is largest for the Hβ line, which has a minimal RV amplitude of 91 m s^{-1}, and gradually decreases for lines showing higher amplitudes. It will be shown in a following paper that this gradual change in phase lag is probably connected with line formation in the atmosphere.

6. Radial velocity variations of individual elements

For all measured lines we did a period search with the periodogram method. This analysis allowed us to crudely estimate the probability that a given period is true (Horne & Baliunas 1986). They developed an algorithm which applies to fully resolved frequency spectra. The results – RV amplitudes with the error, period and error, and probability of the period – are given in Table 4 (Online Material). HJD = 2 453 320.0 was chosen as a reference time for our pulsation analysis. It is remarkable that the weighted mean from all periods with a probability higher than 0.99 determined from individual lines yields exactly the value of the most prominent photometric period observed in 2000–2004, which is $P = 6.125$ min.

The large number of measurable lines of different chemical species allows for a detailed analysis of pulsation waves in the atmosphere of HD 24712, but which will be presented in a follow up paper. Here we discuss briefly pulsation properties derived for different chemical elements.

- *Hydrogen*: Hγ, Hβ and Hα cores indicate pulsation with the amplitude increasing from Hγ to Hα. Our measurements support the results obtained by Balona & Laney (2002) for α Cir and by Balona (2002) for HR 3831, and all together they provide a direct evidence for the growth of pulsation amplitudes towards the upper atmospheric layers. Bisector measurements of the Hα line are shown in Fig. 4 (RV amplitudes – right panel, phases – left panel). Both, amplitudes and phases increase with line depth, i.e. towards the upper atmospheric layers as is observed also in other roAp stars (for example α Cir, Baldry et al. 1999; γ Equ, Sachkov et al. 2004a; or HD 99563, Elkin et al. 2005).
- *Na, Mg, S and Si*: lines of these elements do not reveal any pulsation. The upper limit for the RV amplitudes ranges from 10 to 30 m s^{-1}, depending on the line strength and hence accuracy of measurements. Bisector measurements across the Mg I 5172 Å line (Fig. 5) also rejects variability with an amplitude above 40 m s^{-1}. With the exception of the bisector close to the continuum ($r = 0.96$) we never recover the true pulsation period in a periodogram. The pulsation signal at $r = 0.96$ is explained by a La II blend in the red wing of the Mg I line. A significant pulsation amplitude was also measured in the 4696.20 Å line, which coincides with a S I feature, but which may be attributed to an unclassified Nd III line at λ 4696.205 Å. The latter information is from the unpublished lists of Crosswhite (1976) which were the main source for official NIST data on Nd III energy levels (Martin et al. 1978).
- *Fe-peak elements*: about half of the measured Ca lines show oscillations compatible with the photometrically observed pulsation periods. In four cases we found a signal with 96% significance, among which is the core of the resonance Ca II 3933 Å line, obviously formed high in the atmosphere. Bisector measurements across the Ca I 6122.22 Å line are shown in Fig. 5.

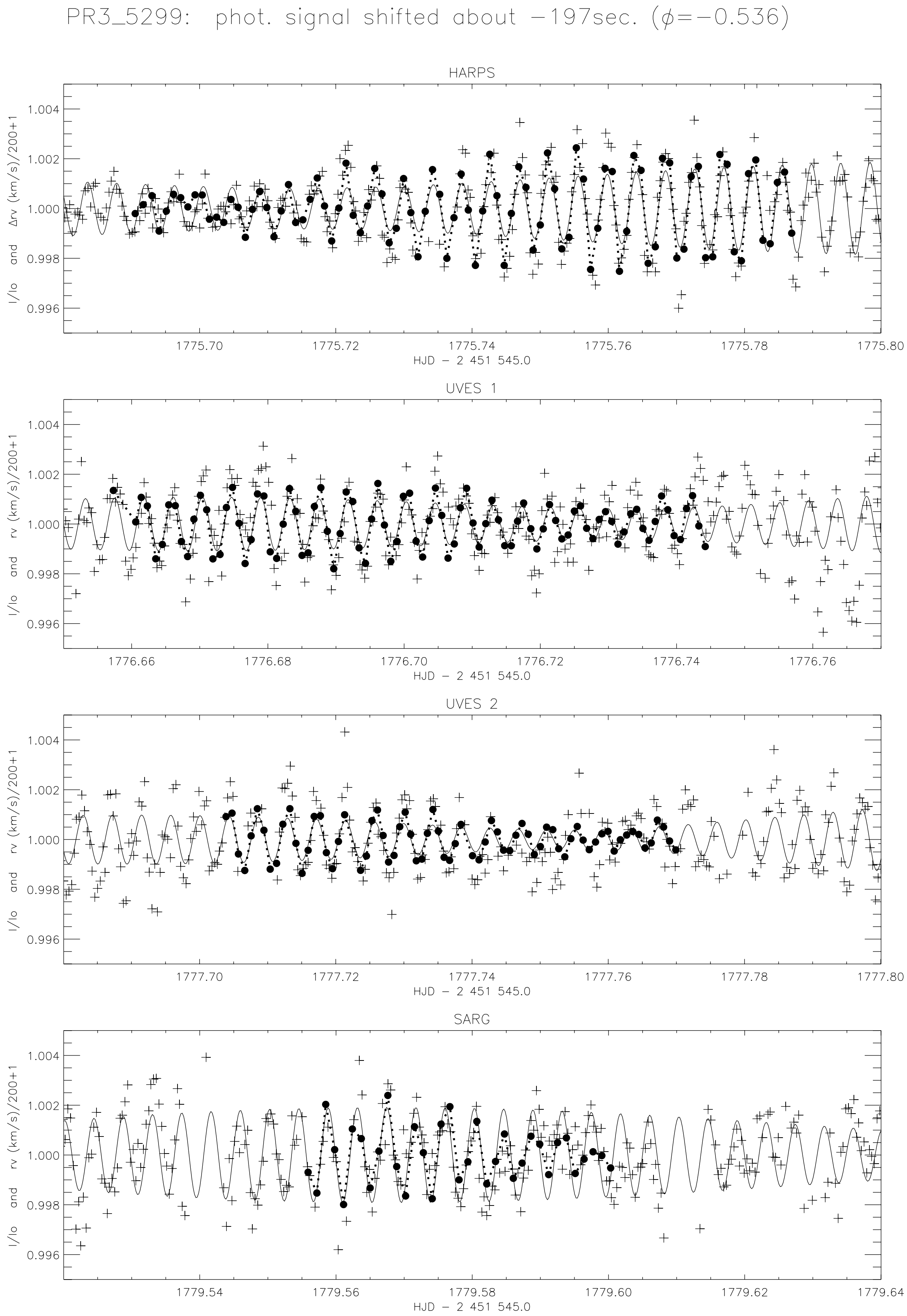

Fig. 3. Normalized RV variations for Pr III (filled circles) are compared with a synthetic light curve (black solid line, computed with the three largest amplitude frequencies derived from the entire MOST observing run) and with simultaneous MOST photometric data (crosses). The dotted line connects the Pr III 5299 Å spectral line RV values (dots) and it follows well the solid line, based on MOST photometry.

Table 3. Phase lag in seconds between luminosity and RV variations for different chemical species. The fourth column gives the same phase lags based on a pulsation period of 6.125 min.

Line	λ (Å)	Phase lag in seconds	Phase lag in periods
Hβ	4861	-356 ± 25	-0.97 ± 0.08
Eu II	6645	-356 ± 22	-0.97 ± 0.06
Nd II	6650	-313 ± 22	-0.85 ± 0.06
Hα	6563	-307 ± 22	-0.84 ± 0.06
Nd III	5286	-301 ± 21	-0.82 ± 0.06
Nd II	5255	-297 ± 21	-0.81 ± 0.06
Nd III	6690	-294 ± 22	-0.80 ± 0.06
Nd III	5851	-283 ± 22	-0.77 ± 0.06
Dy III	5730	-278 ± 22	-0.76 ± 0.06
Nd III	5845	-270 ± 21	-0.73 ± 0.06
Nd III	5203	-255 ± 21	-0.69 ± 0.06
Nd III	5294	-247 ± 22	-0.67 ± 0.06
Pr III	5300	-197 ± 21	-0.54 ± 0.06
Tb III	5505	-104 ± 22	-0.28 ± 0.06

Although this line indicates weak variation with a period of 6.125 min (and a probability of 0.82%), the bisector variations do not differ from those of constant Mg I and Fe II lines. A small unknown blend of a REE would be enough to produce a spurious, very low amplitude variation in even a strong, but non-pulsating line (see below).

Three out of 5 Sc II lines show pulsation, but they all are blended with REE lines. Similarly, nine out of 21 measurable Ti lines show small amplitude variations with the known pulsation period. The Ti II 4501.26 Å line is blended with Nd III 4501.23 Å which contributes to about 25% of the total line intensity, thus resulting in the pulsation signal with the typical phase of Nd lines.

Cr, Mn, Fe, and Co lines do not pulsate. Only 25% of the whole set of measured lines have pulsation periods typical for HD 24712, and part of these lines are blended with lines of REEs. Figure 6 displays RV amplitudes derived from sine-fits to lines of Fe-peak elements with a pulsation period of 6.125 min, and as a function of central residual intensities. We can conclude the absence of pulsation with amplitudes exceeding 15 m s^{-1} in the whole atmospheric range where Fe-peak lines are formed. An apparent increase of the RV amplitude for weaker lines simply reflects a reduced accuracy of the measurements.

A few lines of the Fe-peak elements have rather large RV amplitudes (triangles in Fig. 6) and in most cases this is a result of blending with a REE. Two spectral lines at 5208 Å and 5429 Å are of particular interest, because they are usually identified as Cr I and Fe I lines, respectively, and their pulsation characteristics attributed to these elements (e.g., Elkin et al. 2005). Actually, these lines are heavily blended with Pr III 5208 Å and Nd III 5429 Å, respectively, and consequently show typical REE pulsation phases, but with reduced amplitudes.

- *Sr to Ba*: spectral lines of Sr, Y, Zr, Rh, Pd, In and Ba were measured in the spectrum of HD 24712. Five Ba II lines are constant to within 10 m s^{-1}, as are also lines of Rh I and Pd I. A spectral feature at λ 4511.26 Å, identified as In I 4511.31 Å, may be blended with an unclassified line of Ho (Crosswhite 1976). Pulsation is seen in Sr II lines and in five out of 11 lines of Y II. We carefully checked for blends and can exclude this possibility as explanation for a pulsation signal. Pulsation does not appear in weaker lines of Y II and there is a definite dependence of the RV amplitude and phase on line intensity. It seems that Y II lines originate in the atmosphere where lines with high pulsation amplitudes just start to be formed.
- *Rare Earth elements*: we have measured 260 lines of 13 REEs in the first and the second ionization stage. Almost all of them show pulsation with large amplitudes and different pulsation phases, depending on the species and line intensity (see also Table 3). Bisector measurements at different (continuum normalized) intensity levels of two representative lines, Nd III 5294 Å and Pr III 5300 Å, are shown in Fig. 4. Although RV variations are present, they are not as large as in the roAp star γ Equ (Sachkov et al. 2004a). No difference in the pulsation signature is found for lines of the same element/ion located on both sides of the Balmer jump. For example, two Nd III spectral lines, λ 3603 and λ 6145 Å, formed at approximately the same depth in the stellar atmosphere according to Mashonkina et al. (2005) have RV amplitudes of 185 and 194 m s^{-1}, and pulsation phases of 0.74 and 0.79, respectively (data set 13, UVES).
- *Thorium*: two lines identified as Th III were measured, but no significant pulsation was detected. Using equivalent width measurements and the model atmosphere from Ryabchikova et al. (1997), we estimate a Th abundance of $\log(\mathrm{Th}/N_{\mathrm{tot}}) = -9.26 \pm 0.12$. Oscillator strengths for Th III lines were taken from Biémont et al. (2002). The thorium abundance in HD 24712 is comparable to that in HD 101065 (Cowley et al. 2000), and the thorium overabundance in the atmosphere is similar to the overabundance of most REE obtained from the first ions. Note, that Th abundance in both stars, HD 24712 and in HD 101065 has been derived using partition functions (PF) from Kurucz' ATLAS9 code.
- *Unidentified lines*: along with lines of well established identification we measured all unidentified features with equivalent width $\geq$10 mÅ. The total number of these lines is 115, and about one third of them coincide with the position of Nd III lines from Crosswhite's unpublished list. Because they are not yet classified, we consider them as unidentified lines requiring a proper identification. Most of these potential Nd III lines have pulsation phases in the range of 0.4 to 0.5, corresponding well to the classified Nd III lines. Only one line at λ 4748.17 Å does not show pulsation variations, all other lines reveal pulsation with the typical amplitudes and phases of REEs. We conclude that plenty of still unknown REE lines are present in the spectra of roAp stars.

The ability to constrain classification of unidentified lines on the basis of their pulsation amplitudes and phases and thus provide useful information for laboratory studies is worth mentioning. This is a unique property of roAp stars, and it was already used in the classification study of the Nd III lines (Ryabchikova et al. 2006).

7. Discussion

We have obtained time-resolved observations with different spectrographs in different years (2001, 2003 and 2004) and at nearly the same rotation phases close to the magnetic maximum. We have already reported the similarity of phase shifts between RV variations in the lines of different elements/ions (Sachkov et al. 2004b) based on the observations taken in 2001 and 2003. Figure 7 gives another comparison of the RV variations derived from the observations taken in 2001 (GECKO) and in 2004 (HARPS) at rotation phase 0.87. It was mentioned in Sect. 4 that the frequency analysis of our observations in 2001 and 2004 reveals the same highest amplitude frequencies of 2720.9 and 2652.9 μHz, which corresponds to pulsation periods

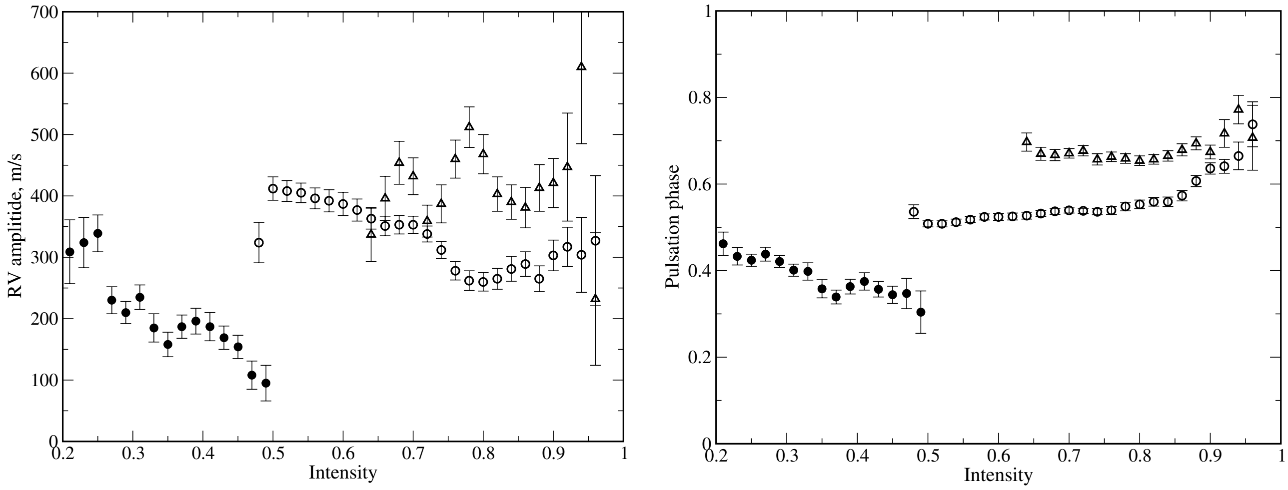

Fig. 4. Bisector measurements of the Hα line (filled circles), lines of Nd III 5294 Å (open circles), Pr III 5300 Å (open triangles). (crosses). The RV amplitudes are shown in the *left panel* and pulsation phases (based on P = 6.125 min) in the *right panel*.

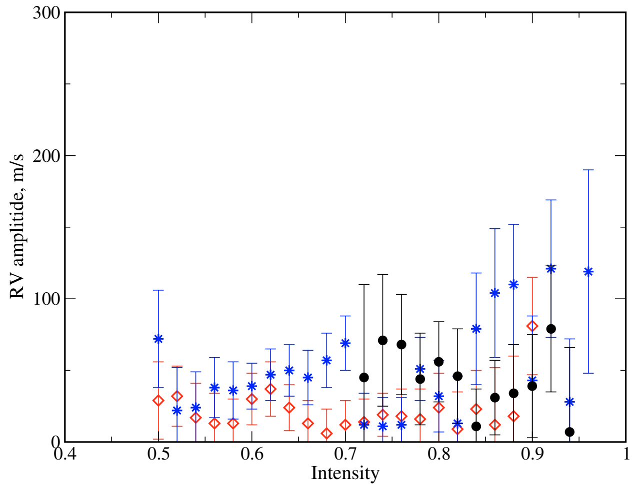

Fig. 5. Bisector RV amplitudes (based on P = 6.125 min) of Fe II 5169 Å (open diamonds), Mg I 5172 Å (asterisks), and Ca I 6122 Å (filled circles).

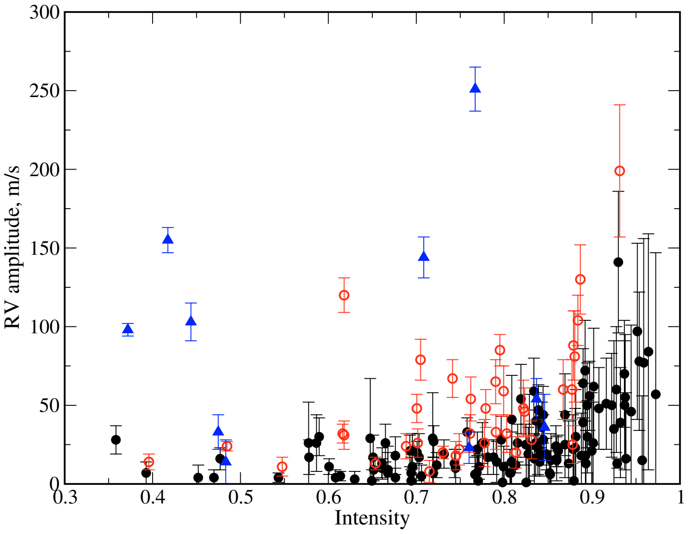

Fig. 6. Pulsation amplitude versus central residual intensity for lines of Fe-peak elements. Filled/open circles indicate lines with no pulsation/known pulsation period, respectively. Fe-peak lines known to be blended with the REEs are marked with triangles.

of 6.125 and 6.28 min. In 2003 we got only 53 spectra and hence we can not resolve frequencies, therefore a mean period of 6.20 min was used. RV amplitudes and phases for a sample of common lines observed in 2001, 2003 and 2004 are given in Table 5 (Online material). Phases in 2001 and 2003 were calculated relative to the HJD of the first observation in a given year and were shifted for comparison purpose by –0.1 and –0.2, respectively. Obviously, the same lines are variable and the similarity of amplitudes and phases of the RV maximum indicate stability of the pulsation pattern in the atmosphere of HD 24712 at least during recent years.

Simultaneous photometry and spectroscopy allow us for the first time to phase accurately RV variations due to pulsation observed in different spectral lines with the photometric pulsation signature. To determine a phase shift between RV and light variations we used the pulsation frequency with the largest photometric amplitude in the WET and MOST data (6.125 min).

Our results show a gradual decrease of the phase lag from the Hβ line to Tb III lines, which may be interpreted as a running wave in the atmosphere of HD 24712, if different lines are formed at different atmospheric layers. The same phenomenon, known as the Van Hoof effect, was found earlier in β Cep-type stars (Mathias & Gillet 1993) and allowed them to derive the propagation time of the running wave through the stellar atmosphere. A first estimate of the running pulsation wave speed in the atmosphere of HD 24712 can be obtained from the phase lags and the respective formation depths of the Nd II and Nd III lines determined according to Mashonkina et al. (2005). In the relevant atmospheric layers ($-6.2 \leq \log \tau_{5000} \leq -4.2$) the pulsation wave propagates with nearly constant speed of ~6 km s^{-1} which is slightly less than the sound speed in adiabatic approximation.

An analysis of the running wave properties in a roAp star atmosphere is rather difficult. First, we know that elements are stratified in the atmospheres of Ap and roAp stars (Babel 1992; Ryabchikova et al. 2002, 2005a), and therefore stratification has to be taken into account for the line formation depth calculations. Second, a stratification analysis of the REEs, which are the main carriers of pulsation information, is not correct without considering NLTE effects (Mashonkina et al. 2005). The third important issue is the surface inhomogeneity in the chemical composition. HD 24712 is a spectrum variable and the first rough analysis of the element distribution was published by Preston (1972). Later, Ryabchikova et al. (2000) showed evidence for a concentration

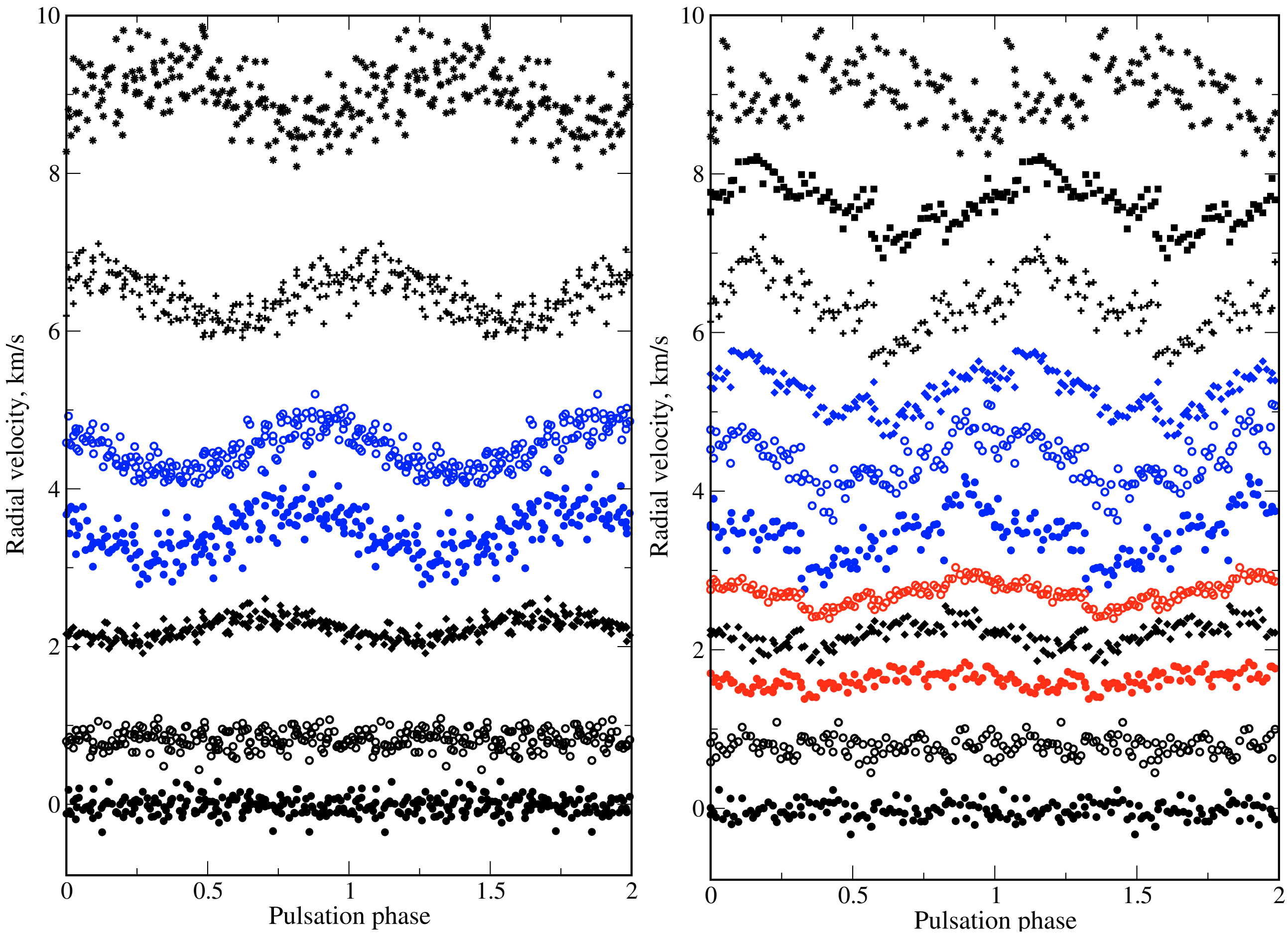

Fig. 7. Radial velocity variations with a period of $P = 6.125$ min for selected spectral lines in 2001 (*left panel*) and in 2004 (*right panel*). In the right panel lines from bottom to top are: Ca I 6717, Fe I 6678, Hβ (core), Eu II 6645, Hα (core), Nd II 6650, Nd III 6690, Nd III 6550, Pr III 6706, Er III 4735, and Tb III 6688 Å. Same lines except of Hβ (core), Hα (core), Nd III 6550, and Er III 4735 are displayed in the *left panel*.

of the Fe-peak elements in a wide band around the magnetic equator, while REEs (in particular Pr and Nd) and Co are concentrated in large spots near, but not exactly at one magnetic pole (the other pole is never visible). Our magnetic field measurements support this difference in the element surface distribution.

Recent Magnetic Doppler Imaging of HD 24712 (Lüftinger et al. 2006) revealed a small but non negligible difference (both in longitude and latitude) between the surface distributions of different REE elements. Therefore, part of the phase shifts between RV curves *may* be due to the different chemical surface distribution relative to the magnetic pole. Cunha (2006) showed that phase shifts may reach 0.25 of the period between the magnetic pole and the magnetic co-latitude $\theta \sim 30°$ (see lower panel of Fig. 6 in Cunha 2006).

A detailed study of the line formation depth in the atmosphere of HD 24712 will be subject of a forthcoming paper. However, some first information may be obtained already without such a detailed analysis when plotting the maximum RV value observed for a given spectral line as a function of pulsation phase, determined from photometry. If the photometric pulsation phase of the maximum RV is related to specific line-forming layers in the stellar atmosphere, then we expect new insights in a pulsating atmosphere. Figure 8 shows RV amplitudes as a function of pulsation phases for numerous lines of several elements measured in UVES spectra (rotation phase 0.944). These pulsation data include bisector measurements of the Hα core and the cores of Ca I and Ca II resonance lines.

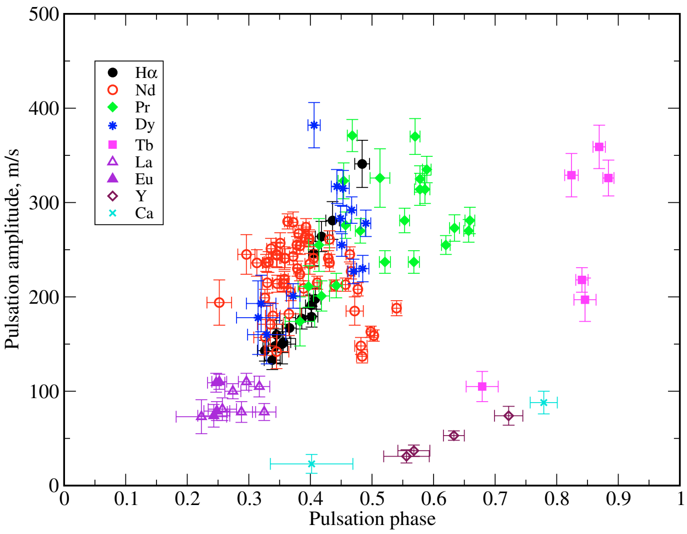

Fig. 8. Pulsation amplitude of spectral lines versus pulsation phase at RV maximum, based on a pulsation period of 6.125 min.

The data seem to cluster along two curves separated roughly by 0.5 of a pulsation period (Fig. 8). The first curve may be directly connected with optical depth, thanks to NLTE calculations for hydrogen and Nd lines (Mashonkina et al. 2005; Sachkov et al. 2006). The RV amplitude grows towards the upper layers, reaches a maximum and then decreases, as indicated by the Nd and Pr lines.

At present it is difficult to conclude if the second curve represents another part of a continuous amplitude-phase distribution, because it is defined mainly by Y and Tb lines, which formation depths are unknown. We think that Tb lines are formed at about the same depth or higher than Nd, Pr and other REE lines. The core of the resonance Ca II 3933 Å line (pulsation phase of 0.8) may be also formed high in the atmosphere, particularly if one considers possible stratification of Ca. But the Y lines are probably formed in lower atmospheric layers.

Our observations allow us to check the claimed pulsation phase jumps of 180° at rotation phases corresponding to magnetic extrema (Mkrtichian & Hatzes 2005). These authors had to link two sets of observations, separated by one month (more than 9000 pulsation cycles), to cover these phases. The phase jumps reported by Mkrtichian & Hatzes occur exactly between the two sets of observations. We, on the other hand, do not observe any phase changes exceeding 35° (0.1 of the pulsation period) in our data sets, which fortunately happen to cover in 2002 the magnetic minimum in 4 consecutive nights (sets 4 to 10) and in 2004 the magnetic maximum in 4 nights of which three were consecutive (sets 12 to 15). Thus, we believe that the rotational modulation of pulsation phase reported for HD 24712 by Mkrtichian & Hatzes (2005) is spurious.

Finally we want to point again to Table 4 which provides the basis for the present investigation. It is a compilation of unblended spectral lines measured in the spectral range from λ 3900 to 6800 Å and of further 80 lines bluewards the Balmer jump. Because of its volume this table is available only as online material. We present the measured central wavelengths of nearly 600 spectral lines in Å, followed by the pulsation amplitude in m s^{-1} and the amplitude error, the period with the largest amplitude determined with a least-squares fit after a periodogram analysis and the probability of the given period (Horne & Baliunas 1986). The next four columns give amplitude, amplitude error, phase relative to the main photometric period observed by MOST (6.125 min) and the phase error. These data are followed by the same information, but relative to the third prominent photometric period observed by MOST (6.282 min), which is the second prominent spectroscopic period. And finally we give in the last column additional information. This table includes information of pulsation properties of ~600 spectral lines in the roAp star HD 24712 observed in 2004 in a range of more than 3000 Å. Because of the known rotational modulation of the pulsation RV amplitudes (see Fig. 3) the lines measured in both observing runs have different amplitudes in Table 4.

8. Conclusions

An extensive spectroscopic and polarimetric study of HD 24712 provide new information about the pulsation properties of a roAp star atmosphere. With this new analysis we confirm our previous results (Sachkov et al. 2004b) and of Balona & Zima (2002), that REE lines and the Hα core show large pulsation amplitudes (150 to 400 m s^{-1}), while spectral lines of the other elements (Mg, Si, Ca, Fe-peak) are nearly constant.

Our data permit for the first time to determine directly the phase shifts for different chemical elements, respectively ions, between pulsation signatures observed in RV data and in photometry. These shifts, derived from contemporaneous photometric and spectroscopic observations, together with magnetic field measurements over a stellar rotation period, will be used in our forthcoming structural analysis of the pulsating atmosphere of HD 24712.

Acknowledgements. We thank the MOST Science Team for providing us with the photometric data and frequency analysis of HD 24712 prior to publication. This work was supported by the Austrian FFG-ALR (MOST Ground Station) and Austrian Science Fund (FWF-P17580N2), by grant 11630102 from the Royal Swedish Academy of Sciences, and by the Natural Sciences and Engineering Research Council of Canada. T.R. and M.S. acknowledge financial support from RFBR grant 04-02-16788a and from the RAS Presidium (Program "Origin and Evolution of Stars and Galaxies"). We also thank our referee, Don W. Kurtz, for his constructive comments which helped to improve the paper.

References

Aldenius, M. 2001, Master Thesis, Depart. of Physics, Univ. of Lund
Babel, J. 1992, A&A, 258, 449
Baldry, I. K., Viskum, M., Bedding, T. R., et al. 1999, MNRAS, 302, 381
Balona, L. A. 2002, MNRAS, 337, 1059
Balona, L. A., & Zima, W. 2002, MNRAS, 336, 873
Balona, L. A., & Laney, C. D. 2003, MNRAS, 344, 242
Biémont, E., Palmeri, P., & Quinet, P. 1999, Ap&SS, 635, 269
Biémont, E., Palmeri, P., Quinet, P., Zhang, Z. G., & Svanberg S. 2002, ApJ, 567, 1276
Crosswhite, H. 1976, unpublished data
Cowley, C. R., Ryabchikova, T., Kupka, F., et al. 2000, MNRAS, 317, 299
Cunha, M. S. 2006, MNRAS, 365, 153
Cunha, M. S., Fernandes J. M. M. B., Monteiro, M. J. P. F. G. 2003, MNRAS, 343, 831
Elkin, V. G., Kurtz, D. W., & Mathys, G. 2005, MNRAS, 364, 864
Horne, J. H., Baliunas, S. L. 1986, ApJ, 302, 757
Ilyin, I. V. 2000, High resolution SOFIN CCD échelle spectroscopy, Ph.D. Thesis, University of Oulu
Kochukhov, O. 2006, in Magnetic Stars, ed. I. I. Romanyuk, & D. O. Kudryavtsev, in press
Kupka, F., Piskunov, N., Ryabchikova, T. A., Stempels, H. C., & Weiss, W. W. 1999, A&AS, 138, 119
Kurtz, D. W. 1982, MNRAS, 200, 807
Kurtz, D. W., Kawaler, S. D., Riddle, R. L., et al. 2002, MNRAS, 330, L57
Kurtz, D. W., Cameron, C., Cunha, M. S. et al. 2005, MNRAS, 358, 651
Leone, F., & Catanzaro, G. 2004, A&A, 425, 271
Lüftinger, T., Kochukhov, O., Ryabchikova, T., Weiss, W. W., & Ilyin, I. 2006, in Magnetic Stars, ed. I. I. Romanyuk and D. O. Kudryavtsev, in press
Martin, W. C., Zalubas, R., & Hagan, L. 1978, NSRDS-NBS 60, Washington
Mashonkina, L. I., Ryabchikova, T. A., & Ryabtsev, A. N. 2005, A&A, 441, 309
Mathias, P., & Gillet, D. 1993, A&A, 278, 511
Matthews, J. M., Wehlau, W. H., Walker, G. A. H., & Yang, S. 1988, ApJ, 324, 1099
Mkrtichian, D. E., & Hatzes, A. P. 2005, A&A, 430, 263
Preston, G. W. 1972, ApJ, 175, 465
Piskunov, N. E. 1999, in 2nd International Workshop on Solar Polarization, ed. K. Nagendra, & J. Stenflo, (Kluwer Acad. Publ.) ASSL, 243, 515
Ryabchikova, T. A., Landstreet, J. D., Gelbmann, M. J., et al. 1997, A&A, 327, 1137
Ryabchikova, T. A., Tsymbal, V. V., Malanushenko, V. P., & Savanov, I. S. 2000, in Magnetic Fields of Chemically Peculiar and Related Stars, ed. Yu. V. Glagolevskij, & I. I. Romanyuk, Moscow, 180
Ryabchikova, T., Piskunov, N., Kochukhov, O., et al. 2002, A&A, 384, 545
Ryabchikova, T., Leone, F., & Kochukhov, O. 2005a, A&A, 438, 973
Ryabchikova, T., Wade, G. A., Auriére, M., et al. 2005b, A&A, 429, L55
Ryabchikova, T., Ryabtsev, A., Kochukhov, O., & Bagnulo, S. 2006, A&A, 456, 329
Sachkov, M., Ryabchikova, T., Kochukhov, O., et al. 2004a, in Variable Stars in the Local Group, ed. D. W. Kurtz, & K. R. Pollard, ASP Conf. Ser., 310, 208
Sachkov, M., Ryabchikova, T., Ilyin, I., et al. 2004b, in The A-Star Puzzle, ed. J. Zverko, W. W. Weiss, J. Žižňovský, & S. J. Adelman (Cambridge University Press), IAU Symp., 224, 770
Sachkov, M., Ryabchikova, T., Bagnulo, S., et al. 2006, in Stellar Pulsation and Evolution, ed. A. R. Walker, G. Bono, Mem. Soc. Astron. Ital., 77, 397
Tsymbal, V., Lyashko, D., & Weiss, W. W. 2003, in Modelling of Stellar Atmospheres, ed. N. Piskunov, W. W. Weiss, D. F. Gray, ASP, IAU Symp., 210, E49
Walker, G., Matthews, G., Kuschnig, R., et al. 2003, PASP, 115, 1023

Online Material

Table 4. Summary of our spectroscopic pulsation analysis of individual spectral lines in HD 24712. The columns give central wavelengths in Å, followed by the pulsation amplitude A (in m s^{-1}), its error σ_A and the period P (in min) with the respective error estimate σ_P derived with a least-squares fit. Corresponding probability of periodic signal (Prob., calculated according to Horne & Baliunas 1986). The next two groups of columns give pulsation amplitudes and phases ϕ with the respective errors, determined with a simultaneous fit of two fixed pulsation periods indicated in the column head.

Wavelength	Free period					Fixed periods								Identification
						6.125 min				6.282 min				
Å	A (m s^{-1})	σ_A	P (min)	σ_P	Prob.	A (m s^{-1})	σ_A	ϕ	σ_ϕ	A (m s^{-1})	σ_A	ϕ	σ_ϕ	
Hydrogen														
HARPS														
4340.468	59	15	6.237	0.041	0.847	22	18	0.132	0.132	44	18	0.759	0.067	Hγ
4861.330	91	11	6.115	0.018	1.000	93	13	0.230	0.022	39	13	0.605	0.053	Hβ
6562.799	175	10	6.140	0.009	1.000	168	8	0.376	0.008	87	8	0.785	0.015	Hα
Na														
HARPS														
5895.996	37	12	3.831	0.018	0.368	30	14	0.581	0.077	20	14	0.656	0.118	Na I
Mg														
HARPS														
5172.701	22	6	3.862	0.017	0.644	20	7	0.656	0.062	14	7	0.759	0.088	Mg I
Si														
HARPS														
5701.115	113	40	5.501	0.043	0.122	35	50	0.209	0.069	43	49	0.343	0.025	Si I
5056.005	20	7	3.426	0.018	0.053	5	9	0.612	0.134	5	9	0.690	0.119	Si II
5978.939	82	23	4.418	0.022	0.700	89	28	0.558	0.051	66	28	0.707	0.069	Si II
6347.113	41	10	9.187	0.086	0.907	29	13	0.371	0.071	37	13	0.567	0.055	Si II
S														
HARPS														
4696.202	316	35	6.126	0.017	1.000	304	39	0.405	0.020	160	38	0.813	0.039	S I+ Nd III 4696.205
Ca														
HARPS														
4226.735	27	8	10.281	0.123	0.481	21	9	0.548	0.073	9	9	0.781	0.156	Ca I core
4425.444	16	5	6.207	0.049	0.388	11	6	0.356	0.087	11	6	0.849	0.091	Ca I
5349.471	25	7	3.302	0.014	0.616	13	9	0.246	0.117	5	9	0.428	0.119	Ca I
5590.124	34	13	3.065	0.016	0.376	2	16	0.535	0.147	14	15	0.759	0.020	Ca I
5857.467	30	9	8.749	0.094	0.503	21	11	0.313	0.087	24	11	0.622	0.075	Ca I
5867.564	147	36	5.794	0.033	0.925	141	45	0.227	0.051	47	45	0.403	0.152	Ca I bl.?
6122.224	28	7	6.149	0.040	0.825	26	9	0.211	0.055	14	9	0.632	0.098	Ca I
6162.198	34	10	4.562	0.024	0.574	18	12	0.506	0.106	12	12	0.129	0.156	Ca I
6163.760	63	22	4.329	0.026	0.149	18	27	0.311	0.076	42	27	0.138	0.102	Ca I
6439.107	30	7	6.175	0.038	0.926	24	8	0.470	0.057	18	8	0.921	0.076	Ca I
6462.592	21	6	6.221	0.046	0.568	8	7	0.105	0.147	15	7	0.665	0.080	Ca I
6471.673	56	13	6.082	0.035	0.941	59	16	0.346	0.043	30	16	0.692	0.085	Ca I
6493.793	48	12	6.116	0.038	0.896	54	14	0.825	0.044	18	15	0.128	0.125	Ca I
6499.655	26	8	10.094	0.132	0.303	19	10	0.978	0.090	5	10	0.420	0.155	Ca I
6717.705	53	55	3.060	0.027	0.005	26	19	0.227	0.118	46	19	0.354	0.067	Ca I
3933.655	126	21	6.134	0.025	0.999	121	25	0.816	0.033	43	25	0.243	0.093	Ca II core
5021.158	52	16	3.952	0.019	0.423	2	20	0.104	0.046	14	20	0.840	0.063	Ca II
5285.280	51	16	6.112	0.047	0.411	60	19	0.842	0.052	26	19	0.878	0.120	Ca II
Sc														
HARPS														
4415.579	143	12	6.135	0.013	1.000	130	14	0.366	0.017	55	14	0.829	0.041	Sc II + Nd III 4415.60
5239.807	251	17	6.135	0.010	1.000	251	14	0.396	0.009	139	14	0.781	0.016	Sc II + Ce II 5239.84
5526.831	53	11	6.027	0.031	0.986	54	13	0.397	0.040	35	13	0.708	0.063	Sc II + Ce II 5526.86
5641.007	516	358	3.049	0.006	0.354	84	75	0.340	0.141	87	74	0.313	0.139	Sc II
5657.908	80	20	9.500	0.092	0.854	26	26	0.267	0.001	37	26	0.423	0.116	Sc II + Fe II
Ti														
UVES1														
3444.295	114	14	6.113	0.020	1.000	111	18	0.229	0.026	35	18	0.494	0.081	Ti II + Dy II 3444.25
3491.039	58	9	6.096	0.028	0.999	63	12	0.065	0.032	23	12	0.384	0.083	Ti II
HARPS														
4518.038	96	32	5.122	0.035	0.237	55	40	0.055	0.116	4	40	0.666	0.075	Ti I
4913.636	108	33	3.427	0.014	0.493	15	41	0.865	0.098	35	41	0.680	0.026	Ti I
5016.182	117	36	3.934	0.018	0.462	78	44	0.511	0.091	50	45	0.522	0.141	Ti I
4422.380	25	8	3.679	0.018	0.223	21	10	0.039	0.077	3	10	0.294	0.045	Ti II
4464.470	29	5	6.061	0.025	0.999	32	6	0.990	0.030	12	6	0.273	0.075	Ti II
4501.267	94	6	6.118	0.010	1.000	98	4	0.436	0.008	53	4	0.799	0.014	Ti II + Nd III 4501.23
4529.513	13	5	7.566	0.082	0.095	10	6	0.002	0.096	3	6	0.467	0.121	Ti II
4563.774	30	3	6.177	0.018	1.000	24	3	0.066	0.025	19	3	0.514	0.032	Ti II
4583.409	90	24	6.083	0.039	0.820	81	29	0.387	0.056	17	28	0.910	0.102	Ti II
4708.683	37	13	9.331	0.119	0.086	28	15	0.797	0.088	9	15	0.415	0.102	Ti II
4805.105	35	8	6.149	0.033	0.976	31	9	0.225	0.048	14	9	0.693	0.107	Ti II
4911.212	27	8	8.466	0.085	0.581	33	9	0.957	0.046	19	9	0.167	0.077	Ti II
5005.194	63	19	7.388	0.067	0.449	30	23	0.275	0.124	44	23	0.801	0.086	Ti II
5013.706	56	13	8.238	0.061	0.974	35	16	0.181	0.074	16	16	0.471	0.005	Ti II
5129.176	22	6	3.418	0.013	0.845	20	7	0.131	0.057	14	7	0.301	0.085	Ti II
5185.918	19	3	6.127	0.028	0.998	20	4	0.977	0.033	12	4	0.338	0.057	Ti II
5226.562	17	4	6.160	0.036	0.937	13	4	0.097	0.058	7	4	0.647	0.111	Ti II
5418.794	58	12	8.912	0.066	0.992	28	16	0.359	0.091	34	16	0.590	0.074	Ti II
6491.602	70	23	8.052	0.085	0.162	51	29	0.951	0.090	30	29	0.056	0.152	Ti II

Table 4. continued.

Wavelength	Free period					Fixed periods								Identification
						6.125 min				6.282 min				
	A	σ_A	P	σ_P	Prob.	A	σ_A	ϕ	σ_ϕ	A	σ_A	ϕ	σ_ϕ	
V														
HARPS														
6119.500	197	78	3.072	0.013	0.122	57	90	0.909	0.091	72	91	0.156	0.038	V I
4564.593	33	9	6.197	0.040	0.855	20	10	0.030	0.082	19	10	0.726	0.090	V II
Cr														
UVES1														
3484.117	35	9	6.119	0.043	0.622	44	12	0.344	0.042	19	12	0.752	0.096	Cr II
HARPS														
4595.598	75	10	6.116	0.021	1.000	85	10	0.396	0.020	59	10	0.726	0.029	Cr I bl?
4600.752	29	9	5.313	0.035	0.483	22	11	0.155	0.079	10	11	0.679	0.005	Cr I
4622.454	49	15	8.124	0.082	0.390	44	18	0.184	0.067	41	18	0.520	0.072	Cr I
4626.191	30	10	3.848	0.020	0.153	26	13	0.927	0.079	20	12	0.211	0.104	Cr I
4637.204	111	15	6.140	0.021	1.000	112	17	0.265	0.025	60	17	0.642	0.047	Cr I
4649.436	57	16	6.100	0.043	0.685	60	19	0.372	0.052	37	19	0.727	0.085	Cr I
4651.294	18	6	5.083	0.036	0.114	11	8	0.055	0.113	12	8	0.298	0.107	Cr I
4652.170	20	5	5.063	0.029	0.768	5	7	0.321	0.033	10	7	0.915	0.112	Cr I
4730.715	41	13	5.365	0.037	0.394	16	16	0.820	0.001	29	16	0.070	0.089	Cr I
4764.305	52	16	3.850	0.019	0.322	13	21	0.403	0.095	29	21	0.662	0.114	Cr I
4771.507	31	10	6.182	0.048	0.283	25	12	0.976	0.075	15	12	0.440	0.123	Cr I?
5208.858	91	11	6.079	0.019	1.000	103	12	0.678	0.020	67	12	0.994	0.030	Cr I, Pr III 5208.51
5247.592	71	21	4.185	0.021	0.561	48	26	0.747	0.087	2	26	0.339	0.014	Cr I
5296.695	46	12	4.407	0.020	0.858	7	15	0.000	0.037	18	15	0.454	0.133	Cr I
5297.379	27	10	3.986	0.023	0.048	1	12	0.652	0.035	8	12	0.504	0.083	Cr I
5348.324	47	15	6.091	0.048	0.354	48	18	0.235	0.061	3	18	0.412	0.152	Cr I
5628.650	209	63	4.912	0.029	0.559	77	79	0.313	0.004	119	80	0.584	0.105	Cr I
4588.206	8	2	3.548	0.016	0.292	4	3	0.025	0.123	8	3	0.198	0.066	Cr II
4592.063	14	4	5.143	0.031	0.508	4	5	0.327	0.027	10	5	0.709	0.082	Cr II
4634.080	11	4	5.978	0.050	0.074	11	5	0.940	0.070	12	5	0.229	0.065	Cr II
5153.502	46	12	6.098	0.040	0.828	46	15	0.148	0.052	14	15	0.535	0.002	Cr II asymm.
5232.513	36	12	5.267	0.037	0.210	7	14	0.503	0.159	30	14	0.933	0.079	Cr II
5237.328	19	5	4.705	0.025	0.694	2	7	0.479	0.086	10	7	0.672	0.107	Cr II
5246.802	44	17	4.987	0.039	0.009	26	21	0.314	0.132	34	21	0.334	0.102	Cr II
5510.720	55	19	3.235	0.013	0.148	22	22	0.712	0.004	31	22	0.048	0.113	Cr II
Mn														
UVES1														
3441.972	15	5	9.739	0.143	0.020	7	7	0.276	0.003	10	7	0.816	0.108	Mn II
3482.887	15	6	4.059	0.028	0.003	16	7	0.259	0.077	9	7	0.682	0.127	Mn II
3488.658	15	6	8.778	0.140	0.000	4	8	0.616	0.133	12	8	0.031	0.109	Mn II
3497.512	29	13	4.460	0.043	0.000	26	18	0.899	0.108	4	18	0.152	0.121	Mn II
HARPS														
4754.052	24	7	5.714	0.040	0.433	19	9	0.911	0.077	15	9	0.110	0.095	Mn I
4761.516	37	11	9.623	0.114	0.478	16	14	0.680	0.143	9	14	0.144	0.093	Mn I
4765.875	59	13	7.456	0.049	0.976	15	17	0.524	0.013	46	17	0.725	0.059	Mn I
4766.430	38	10	6.090	0.039	0.852	33	11	0.320	0.056	26	11	0.754	0.071	Mn I
Fe														
UVES1														
3475.442	26	8	2.864	0.011	0.090	9	11	0.397	0.033	18	11	0.922	0.097	Fe I
3540.099	90	17	6.076	0.032	0.997	89	23	0.342	0.041	11	23	0.952	0.159	Fe I
3581.186	31	8	7.922	0.080	0.134	24	12	0.326	0.075	14	11	0.889	0.128	Fe I
3606.679	29	11	7.489	0.101	0.003	31	24	0.458	0.124	4	24	0.143	0.142	Fe I
3621.464	35	8	6.115	0.042	0.928	38	11	0.868	0.046	20	11	0.161	0.088	Fe I
3621.709	97	36	5.404	0.048	0.036	78	47	0.193	0.097	69	47	0.504	0.109	Fe I
3820.419	12	5	6.517	0.085	0.000	3	7	0.720	0.053	4	7	0.058	0.088	Fe I
4202.039	15	5	6.520	0.069	0.000	16	7	0.640	0.073	11	7	0.036	0.104	Fe I
4213.640	66	7	6.101	0.018	1.000	70	8	0.388	0.020	27	8	0.704	0.052	Fe I
HARPS														
4045.823	49	8	6.107	0.026	0.999	40	8	0.829	0.033	24	8	0.112	0.054	Fe I core
4202.039	19	5	6.164	0.037	0.918	14	5	0.705	0.063	9	5	0.284	0.099	Fe I
4213.640	59	11	6.095	0.027	0.999	67	12	0.451	0.029	50	12	0.774	0.039	Fe I
4484.226	49	8	6.134	0.024	0.999	48	9	0.282	0.031	12	9	0.712	0.118	Fe I
4547.854	44	8	6.245	0.031	0.993	22	10	0.315	0.075	35	10	0.816	0.048	Fe I
4637.522	31	10	6.036	0.047	0.252	32	12	0.442	0.062	12	12	0.662	0.007	Fe I
4668.139	30	7	6.197	0.040	0.899	18	9	0.360	0.081	16	9	0.038	0.091	Fe I
4729.015	130	32	3.805	0.014	0.908	50	41	0.413	0.131	58	41	0.712	0.114	Fe I
4908.043	84	27	4.813	0.031	0.290	70	34	0.480	0.077	33	33	0.856	0.004	Fe I
4909.370	128	19	6.082	0.022	1.000	130	22	0.299	0.028	42	22	0.659	0.084	Fe I bl.
4910.331	23	7	6.855	0.060	0.297	14	9	0.437	0.101	20	9	0.732	0.074	Fe I
4938.833	27	9	7.148	0.071	0.089	7	11	0.345	0.091	7	11	0.197	0.078	Fe I
4950.121	73	18	6.061	0.036	0.920	88	22	0.330	0.039	46	22	0.544	0.074	Fe I bl.?
4966.101	25	9	3.579	0.019	0.054	6	11	0.657	0.147	19	11	0.923	0.097	Fe I
4982.514	23	7	3.476	0.017	0.336	11	9	0.546	0.138	9	9	0.172	0.006	Fe I
5049.834	27	8	5.336	0.034	0.578	7	10	0.052	0.058	18	10	0.071	0.090	Fe I
5051.644	45	10	6.013	0.032	0.982	48	12	0.291	0.040	39	12	0.595	0.048	Fe I
5068.782	25	9	2.927	0.012	0.030	16	11	0.899	0.107	12	11	0.074	0.140	Fe I
5171.615	117	11	6.132	0.014	1.000	120	11	0.391	0.014	69	10	0.763	0.025	Fe I bl.
5196.071	50	17	3.704	0.018	0.176	25	21	0.484	0.133	17	21	0.013	0.036	Fe I
5198.714	56	22	4.901	0.038	0.017	13	27	0.866	0.157	7	27	0.319	0.106	Fe I
5215.202	35	10	5.925	0.042	0.358	14	13	0.251	0.148	28	13	0.431	0.076	Fe I

Table 4. continued.

Wavelength	Free period					Fixed periods								Identification
						6.125 min				6.282 min				
	A	σ_A	P	σ_P	Prob.	A	σ_A	ϕ	σ_ϕ	A	σ_A	ϕ	σ_ϕ	
5217.407	39	13	7.137	0.070	0.135	1	16	0.501	0.020	21	16	0.462	0.126	Fe I
5242.503	32	10	8.150	0.086	0.315	25	13	0.413	0.082	20	13	0.628	0.102	Fe I
5253.477	60	18	7.375	0.067	0.498	56	22	0.220	0.064	15	22	0.304	0.076	Fe I
5281.798	23	8	6.546	0.060	0.122	27	10	0.484	0.058	14	10	0.704	0.113	Fe I
5383.380	29	12	8.747	0.128	0.003	17	14	0.458	0.137	23	14	0.782	0.104	Fe I
5397.142	25	8	3.609	0.018	0.142	13	10	0.922	0.129	25	10	0.164	0.066	Fe I
5405.783	12	4	5.806	0.052	0.020	3	5	0.345	0.147	6	5	0.284	0.143	Fe I
5410.917	15	6	6.852	0.080	0.001	12	8	0.406	0.100	10	8	0.537	0.116	Fe I
5415.211	17	4	5.104	0.030	0.706	4	6	0.046	0.049	5	6	0.227	0.012	Fe I
5424.080	19	6	3.522	0.015	0.413	4	7	0.795	0.124	4	7	0.933	0.133	Fe I
5434.535	23	8	3.376	0.017	0.083	7	10	0.983	0.052	14	10	0.063	0.114	Fe I
5445.050	35	8	6.192	0.036	0.948	23	10	0.185	0.070	20	10	0.945	0.079	Fe I+ Ce II 5445.23
5446.616	40	10	10.376	0.109	0.308	24	13	0.943	0.087	16	13	0.188	0.127	Fe I
5462.968	18	6	3.628	0.017	0.150	7	7	0.262	0.008	3	7	0.597	0.018	Fe I
5466.418	44	13	5.793	0.041	0.520	23	17	0.134	0.118	14	17	0.487	0.031	Fe I
5560.217	106	34	5.406	0.037	0.250	17	42	0.499	0.074	69	42	0.501	0.096	Fe I
5562.712	85	31	5.437	0.043	0.064	62	37	0.290	0.095	53	36	0.767	0.111	Fe I
5576.094	34	10	5.111	0.032	0.488	11	13	0.246	0.027	22	13	0.258	0.095	Fe I
5586.777	28	10	9.075	0.126	0.021	7	13	0.720	0.114	18	13	0.812	0.115	Fe I
5615.656	18	5	7.360	0.067	0.499	9	7	0.574	0.127	7	7	0.884	0.152	Fe I
5775.093	148	44	3.295	0.013	0.445	46	55	0.050	0.033	82	56	0.153	0.107	Fe I
5862.370	70	22	3.457	0.014	0.481	44	26	0.761	0.096	61	26	0.921	0.070	Fe I
5930.195	44	14	4.124	0.022	0.224	40	18	0.741	0.071	19	17	0.743	0.150	Fe I
5987.078	76	22	6.740	0.053	0.536	50	27	0.609	0.086	70	27	0.959	0.062	Fe I
6024.076	40	15	5.019	0.038	0.033	14	19	0.903	0.053	18	19	0.988	0.012	Fe I
6137.714	49	14	3.903	0.017	0.697	19	17	0.208	0.148	5	17	0.739	0.092	Fe I
6191.593	32	10	3.306	0.013	0.363	26	12	0.797	0.075	24	12	0.985	0.081	Fe I
6393.628	35	12	6.662	0.063	0.003	26	15	0.519	0.092	36	14	0.792	0.066	Fe I
6400.024	48	13	6.098	0.040	0.808	47	16	0.151	0.054	7	16	0.583	0.019	Fe I
6411.671	61	21	3.491	0.016	0.081	39	25	0.085	0.106	37	25	0.207	0.111	Fe I
6419.972	82	22	3.282	0.012	0.841	41	28	0.012	0.108	47	27	0.317	0.095	Fe I
6495.004	21	8	7.994	0.094	0.013	6	10	0.408	0.103	7	10	0.008	0.061	Fe I
6678.001	50	21	5.386	0.050	0.000	19	19	0.676	0.001	31	19	0.034	0.100	Fe I
4555.897	12	4	6.472	0.060	0.068	12	5	0.870	0.069	8	5	0.184	0.103	Fe II
4635.331	36	9	4.905	0.024	0.892	33	11	0.364	0.053	14	11	0.723	0.127	Fe II
4923.937	18	3	6.133	0.029	0.997	19	4	0.215	0.034	11	4	0.570	0.056	Fe II+ Nd II 4923.93
4993.357	31	11	3.729	0.020	0.080	14	14	0.077	0.156	14	14	0.207	0.156	Fe II
5018.455	14	2	6.137	0.027	0.996	13	3	0.781	0.038	6	3	0.220	0.082	Fe II+ Ce II 5018.45
5132.675	85	31	4.762	0.033	0.070	29	38	0.229	0.049	44	38	0.985	0.136	Fe II
5169.038	15	4	3.375	0.013	0.796	4	5	0.306	0.013	1	5	0.899	0.012	Fe II
5197.591	11	3	2.933	0.009	0.660	5	3	0.456	0.112	6	3	0.968	0.097	Fe II
5362.838	20	6	3.258	0.015	0.279	15	8	0.556	0.084	19	8	0.714	0.066	Fe II
5414.086	85	31	3.164	0.013	0.084	21	37	0.673	0.115	33	37	0.597	0.019	Fe II
5425.266	55	17	8.390	0.086	0.430	36	21	0.698	0.095	27	21	0.947	0.127	Fe II
6147.747	70	18	6.135	0.040	0.855	64	22	0.960	0.055	24	22	0.417	0.147	Fe II+ Tb III 6147.67
6516.126	27	8	3.416	0.014	0.018	20	10	0.088	0.079	15	10	0.257	0.104	Fe II
6592.934	60	24	2.905	0.013	0.013	29	29	0.296	0.157	12	29	0.433	0.048	Fe II
Co														
UVES1														
3412.622	26	9	4.623	0.034	0.034	30	12	0.289	0.063	19	12	0.835	0.099	Co I
3455.228	26	11	4.566	0.041	0.000	9	15	0.820	0.091	7	15	0.245	0.021	Co I
3489.393	23	8	9.626	0.154	0.016	17	11	0.050	0.104	16	11	0.801	0.109	Co I
3491.296	25	9	4.200	0.029	0.005	26	12	0.430	0.072	26	12	0.770	0.072	Co I
3564.947	30	11	7.690	0.105	0.004	17	15	0.640	0.142	6	15	0.245	0.040	Co I
HARPS														
4588.732	183	35	6.064	0.028	0.998	210	43	0.315	0.033	60	44	0.488	0.115	Co I
4781.449	77	26	4.283	0.026	0.169	50	32	0.691	0.104	63	32	0.898	0.084	Co I
4792.852	23	7	3.333	0.014	0.309	7	9	0.962	0.036	8	9	0.130	0.023	Co I
4813.478	26	8	3.725	0.017	0.304	21	10	0.428	0.079	2	10	0.953	0.100	Co I
4813.969	69	22	2.987	0.009	0.314	23	25	0.756	0.015	13	25	0.590	0.149	Co I
5146.757	28	10	6.037	0.051	0.093	28	12	0.891	0.069	12	12	0.164	0.004	Co I
5254.649	39	9	9.069	0.079	0.944	19	12	0.512	0.102	9	12	0.637	0.044	Co I
5257.615	38	12	6.595	0.058	0.202	11	16	0.610	0.072	6	15	0.292	0.062	Co I
5280.626	25	9	4.160	0.024	0.057	17	11	0.479	0.103	1	11	0.939	0.065	Co I
5342.704	27	9	7.659	0.081	0.125	9	12	0.333	0.036	15	12	0.675	0.122	Co I
5343.395	40	14	3.970	0.022	0.064	6	17	0.808	0.104	32	17	0.591	0.086	Co I
5352.038	32	10	6.132	0.046	0.462	32	12	0.659	0.061	6	12	0.561	0.127	Co I
5444.585	59	18	4.040	0.020	0.424	54	22	0.236	0.066	47	22	0.347	0.076	Co I
5454.576	71	17	8.890	0.074	0.880	59	21	0.176	0.058	53	21	0.403	0.064	Co I
5483.949	80	24	4.346	0.023	0.624	30	30	0.271	0.003	9	30	0.876	0.016	Co I
5489.663	74	27	4.715	0.032	0.063	72	32	0.455	0.072	51	32	0.735	0.102	Co I
5590.734	138	44	4.675	0.028	0.385	35	56	0.741	0.092	55	56	0.995	0.001	Co I
5647.235	79	27	5.365	0.040	0.091	19	34	0.861	0.121	68	34	0.166	0.079	Co I
6257.577	137	48	5.950	0.049	0.115	75	60	0.018	0.127	75	59	0.252	0.128	Co I
6347.833	101	32	7.554	0.071	0.439	60	40	0.874	0.106	5	39	0.906	0.000	Co I
4516.630	81	11	6.132	0.021	1.000	79	12	0.350	0.026	42	12	0.754	0.049	Co II
4569.248	30	10	3.560	0.015	0.361	19	12	0.487	0.097	10	11	0.783	0.033	Co II
4660.636	47	14	6.692	0.055	0.537	44	17	0.367	0.063	17	17	0.600	0.157	Co II
Ni														
UVES1														

Table 4. continued.

Wavelength	Free period					Fixed periods 6.125 min				Fixed periods 6.282 min				Identification
	A	σ_A	P	σ_P	Prob.	A	σ_A	ϕ	σ_ϕ	A	σ_A	ϕ	σ_ϕ	
3515.027	70	10	6.145	0.026	1.000	65	14	0.385	0.033	30	13	0.622	0.074	Ni I
HARPS														
5035.398	80	29	4.155	0.024	0.042	38	35	0.215	0.145	40	35	0.582	0.138	Ni I
Sr														
UVES1														
3380.722	25	8	6.965	0.023	0.817	20	8	0.338	0.061	6	8	0.438	0.038	Sr II
3474.902	114	8	6.116	0.012	1.000	119	10	0.426	0.013	33	9	0.722	0.047	Sr II
HARPS														
4784.335	116	43	3.629	0.019	0.069	47	51	0.623	0.014	111	51	0.884	0.074	Sr I
4811.889	125	30	9.133	0.081	0.929	27	40	0.469	0.070	27	40	0.541	0.070	Sr I
4215.525	104	7	6.128	0.010	1.000	103	6	0.420	0.010	48	6	0.812	0.022	Sr II core
Y														
UVES1														
3549.001	71	9	6.133	0.022	0.999	74	10	0.722	0.023	49	10	0.024	0.035	Y II
HARPS														
5693.659	185	73	10.158	0.166	0.008	119	89	0.282	0.119	132	89	0.694	0.108	Y I
4883.686	82	9	6.092	0.016	1.000	89	10	0.728	0.018	43	10	0.060	0.037	Y II
4982.134	30	10	4.731	0.031	0.116	15	13	0.537	0.136	5	13	0.498	0.082	Y II
5087.427	51	5	6.129	0.016	1.000	52	5	0.693	0.018	27	5	0.075	0.034	Y II
5119.118	28	9	6.044	0.047	0.255	31	11	0.427	0.057	13	11	0.606	0.131	Y II
5289.824	65	19	3.312	0.012	0.626	34	24	0.917	0.110	9	23	0.748	0.072	Y II
5402.781	39	14	3.300	0.016	0.111	24	17	0.563	0.110	29	17	0.024	0.091	Y II
5509.901	30	7	6.049	0.037	0.885	34	9	0.533	0.043	18	9	0.741	0.082	Y II
5662.928	48	7	6.133	0.022	1.000	48	8	0.667	0.027	32	8	0.045	0.040	Y II
5728.899	45	16	3.576	0.018	0.073	20	20	0.360	0.155	17	20	0.539	0.022	Y II
6613.749	85	24	6.195	0.044	0.712	64	29	0.421	0.072	57	28	0.900	0.081	Y II bl.
Zr														
HARPS														
5350.379	168	24	6.189	0.022	1.000	114	29	0.340	0.041	89	29	0.873	0.053	Zr II?
Rh														
UVES1														
3434.865	64	18	3.196	0.014	0.603	18	26	0.420	0.067	22	25	0.679	0.022	Rh I
Pd														
UVES1														
3404.570	14	7	4.807	0.054	0.000	20	9	0.522	0.078	7	9	0.035	0.066	Pd I
HARPS														
5163.819	31	11	3.709	0.020	0.050	6	14	0.580	0.015	15	14	0.670	0.152	Pd I
5295.623	68	23	4.131	0.023	0.202	31	28	0.023	0.146	63	29	0.150	0.072	Pd I
In														
HARPS														
4511.263	254	31	6.173	0.011	1.000	228	36	0.351	0.025	177	36	0.756	0.033	In I
Ba														
HARPS														
4554.032	10	3	3.898	0.017	0.726	9	3	0.871	0.057	6	3	0.237	0.082	Ba II
4934.071	8	2	6.103	0.049	0.298	8	3	0.966	0.063	4	3	0.349	0.116	Ba II
5853.674	19	5	3.697	0.016	0.328	13	7	0.310	0.082	10	7	0.504	0.104	Ba II
6141.718	17	5	3.379	0.013	0.602	11	6	0.841	0.088	5	6	0.485	0.018	Ba II
6496.905	15	4	5.967	0.041	0.592	12	5	0.113	0.071	10	5	0.330	0.086	Ba II
La														
UVES1														
3517.010	88	5	6.110	0.011	1.000	98	6	0.475	0.010	42	6	0.802	0.024	La III
HARPS														
4526.097	113	9	6.160	0.013	1.000	97	10	0.385	0.017	52	10	0.851	0.032	La II
4574.857	113	12	6.164	0.017	1.000	99	13	0.384	0.022	66	13	0.820	0.033	La II
4655.474	155	16	6.118	0.015	1.000	152	17	0.328	0.019	74	17	0.728	0.038	La II
4662.504	151	15	6.108	0.015	1.000	160	14	0.432	0.015	102	14	0.786	0.023	La II
4692.489	107	19	6.119	0.026	0.999	107	23	0.301	0.034	1	23	0.563	0.127	La II
4740.261	170	12	6.140	0.011	1.000	160	11	0.426	0.011	91	11	0.841	0.020	La II
4748.724	134	16	6.162	0.019	1.000	120	18	0.401	0.025	77	18	0.831	0.039	La II
4804.026	123	20	6.095	0.024	0.999	129	23	0.360	0.029	57	23	0.710	0.065	La II
4921.802	146	12	6.133	0.013	1.000	137	12	0.486	0.015	72	12	0.907	0.028	La II
4986.837	82	11	6.141	0.020	1.000	83	11	0.394	0.023	56	11	0.767	0.034	La II
5482.256	128	33	6.078	0.038	0.880	118	40	0.241	0.055	16	40	0.782	0.066	La II
5797.557	93	15	6.103	0.025	0.999	89	18	0.391	0.032	52	17	0.790	0.055	La II
5805.766	159	30	6.087	0.028	0.998	164	36	0.364	0.035	45	36	0.703	0.125	La II
5808.295	144	32	6.101	0.033	0.973	158	38	0.179	0.039	36	38	0.234	0.011	La II
6262.283	183	32	6.150	0.026	0.999	145	38	0.292	0.042	91	37	0.815	0.067	La II + Pr II 6262.55
6296.074	161	30	6.152	0.028	0.999	141	36	0.313	0.041	42	35	0.861	0.137	La II
6320.376	84	13	6.136	0.023	1.000	79	14	0.293	0.030	44	14	0.710	0.053	La II
6399.017	133	42	4.142	0.022	0.339	114	52	0.376	0.073	50	52	0.595	0.005	La II
Ce														
UVES1														
3534.018	233	20	6.138	0.015	1.000	242	23	0.515	0.015	119	23	0.794	0.031	Ce II

Table 4. continued.

Wavelength	Free period					Fixed periods								Identification
						6.125 min				6.282 min				
	A	σ_A	P	σ_P	Prob.	A	σ_A	ϕ	σ_ϕ	A	σ_A	ϕ	σ_ϕ	
3577.444	231	23	6.134	0.017	1.000	250	24	0.504	0.015	172	24	0.816	0.022	Ce II
3395.770	157	47	6.174	0.051	0.589	167	60	0.490	0.058	118	61	0.810	0.081	Ce III+ Ti II 3395.789
3427.352	152	14	6.138	0.016	1.000	146	15	0.590	0.018	88	16	0.857	0.029	Ce III
HARPS														
4418.785	201	11	6.118	0.009	1.000	204	10	0.548	0.008	91	10	0.928	0.018	Ce II
4515.832	111	18	6.131	0.024	0.999	119	18	0.520	0.025	97	18	0.866	0.031	Ce II
4562.357	298	17	6.120	0.009	1.000	299	14	0.549	0.008	142	14	0.934	0.016	Ce II
4591.093	200	19	6.118	0.014	1.000	197	20	0.428	0.016	107	19	0.820	0.030	Ce II
4914.919	199	23	6.102	0.018	1.000	206	26	0.405	0.020	112	25	0.767	0.037	Ce II
5077.853	189	22	6.106	0.017	1.000	201	24	0.461	0.019	91	24	0.805	0.043	Ce II
5147.554	201	31	6.107	0.023	1.000	239	32	0.504	0.022	166	32	0.812	0.032	Ce II
5274.226	288	17	6.126	0.009	1.000	290	16	0.518	0.009	128	16	0.902	0.020	Ce II
5451.102	295	18	6.123	0.009	1.000	298	18	0.377	0.010	120	18	0.761	0.024	Ce II
5468.366	204	26	6.122	0.019	1.000	210	27	0.483	0.021	137	27	0.850	0.032	Ce II
5975.808	165	34	6.105	0.031	0.994	176	39	0.440	0.036	96	39	0.785	0.066	Ce II
6043.372	208	31	6.115	0.023	1.000	214	33	0.497	0.025	158	33	0.862	0.034	Ce II
Pr														
HARPS														
5002.436	272	43	6.120	0.024	0.999	285	48	0.406	0.027	177	47	0.766	0.044	Pr II
5110.759	190	17	6.116	0.013	1.000	199	17	0.468	0.014	106	16	0.828	0.026	Pr II
5129.506	242	20	6.116	0.012	1.000	247	20	0.459	0.013	121	20	0.832	0.027	Pr II
5135.123	305	32	6.094	0.015	1.000	326	34	0.458	0.017	163	34	0.796	0.034	Pr II
5152.243	272	17	6.131	0.009	1.000	265	15	0.412	0.009	120	15	0.818	0.021	Pr II + Nd III 5152.292
5292.598	215	20	6.127	0.015	1.000	208	22	0.472	0.017	109	21	0.877	0.032	Pr II
5343.837	220	66	6.051	0.043	0.580	220	79	0.478	0.057	148	78	0.810	0.086	Pr II + Ce II 5343.90
5681.862	414	78	6.253	0.029	0.998	93	94	0.263	0.002	360	95	0.982	0.042	Pr II
6017.753	255	43	6.115	0.025	0.999	247	49	0.444	0.031	179	48	0.834	0.044	Pr II
6165.922	229	32	6.086	0.020	1.000	254	35	0.481	0.022	155	34	0.803	0.037	Pr II
6584.514	247	62	6.090	0.037	0.925	233	74	0.248	0.051	82	74	0.684	0.143	Pr II
6656.788	320	37	6.090	0.017	1.000	318	45	0.403	0.023	20	45	0.400	0.033	Pr II
6673.390	125	19	6.091	0.022	1.000	135	22	0.380	0.027	45	22	0.692	0.080	Pr II
6673.695	421	46	6.127	0.016	1.000	136	24	0.396	0.029	64	24	0.728	0.061	Pr II
4910.816	332	20	6.124	0.009	1.000	334	17	0.572	0.008	158	17	0.955	0.017	Pr III
4929.109	302	20	6.103	0.010	1.000	306	21	0.555	0.011	116	21	0.927	0.030	Pr III
5284.690	345	19	6.132	0.008	1.000	338	11	0.685	0.006	184	12	0.082	0.010	Pr III
5299.986	332	18	6.131	0.008	1.000	327	12	0.678	0.006	173	13	0.074	0.012	Pr III
5339.990	210	16	6.109	0.012	1.000	224	14	0.678	0.010	130	14	0.029	0.018	Pr III bl.
5462.147	167	31	6.127	0.028	0.998	179	38	0.399	0.034	41	38	0.712	0.145	Pr III
5765.251	358	46	6.112	0.019	1.000	337	49	0.556	0.023	226	49	0.963	0.035	Pr III
5844.406	318	18	6.134	0.009	1.000	305	14	0.603	0.008	152	14	0.014	0.015	Pr III
5956.040	307	14	6.122	0.007	1.000	308	9	0.656	0.005	140	9	0.043	0.011	Pr III
5998.935	410	22	6.141	0.008	1.000	382	18	0.606	0.008	188	18	0.035	0.015	Pr III
6052.995	402	23	6.141	0.009	1.000	384	15	0.623	0.006	220	15	0.029	0.011	Pr III
6090.018	372	23	6.126	0.009	1.000	365	18	0.672	0.008	195	19	0.068	0.015	Pr III
6160.238	346	18	6.121	0.008	1.000	342	12	0.657	0.006	172	12	0.051	0.012	Pr III
6195.616	351	19	6.133	0.008	1.000	346	11	0.671	0.005	193	11	0.063	0.009	Pr III
6500.019	386	33	6.128	0.013	1.000	378	35	0.544	0.015	182	35	0.944	0.031	Pr III
6501.488	310	26	6.112	0.012	1.000	325	26	0.584	0.013	154	26	0.940	0.028	Pr III
6578.880	384	33	6.117	0.013	1.000	376	36	0.592	0.016	142	37	0.999	0.041	Pr III
6616.481	314	66	6.193	0.032	0.992	214	79	0.514	0.059	169	80	0.037	0.074	Pr III
6692.225	281	54	6.197	0.030	0.998	245	61	0.547	0.040	230	61	0.929	0.043	Pr III
6706.708	368	27	6.114	0.011	1.000	371	27	0.601	0.012	174	27	0.984	0.025	Pr III
Nd														
UVES1														
3339.057	128	12	6.111	0.016	1.000	131	16	0.379	0.019	42	15	0.662	0.061	Nd II
3375.226	172	18	6.107	0.018	1.000	182	23	0.365	0.020	69	22	0.670	0.053	Nd II
4061.099	156	6	6.117	0.007	1.000	163	6	0.433	0.006	60	6	0.727	0.016	Nd II
4069.270	269	12	6.107	0.007	1.000	290	10	0.389	0.006	115	10	0.704	0.014	Nd II
4211.294	217	14	6.101	0.009	1.000	241	8	0.367	0.006	90	8	0.710	0.015	Nd II
3433.305	28	8	6.128	0.050	0.075	31	11	0.434	0.055	9	11	0.790	0.032	Nd III + Cr II
3442.767	138	11	6.121	0.014	1.000	147	12	0.437	0.014	66	12	0.741	0.030	Nd III
3476.175	137	8	6.109	0.011	1.000	147	10	0.430	0.011	45	10	0.751	0.037	Nd III
3477.830	86	5	6.096	0.012	1.000	99	6	0.454	0.011	40	6	0.819	0.027	Nd III
3537.600	139	10	6.121	0.012	1.000	136	11	0.416	0.013	56	11	0.670	0.033	Nd III + Dy II
3561.860	132	13	6.134	0.017	1.000	134	15	0.394	0.018	66	15	0.666	0.037	Nd III + Ti II
3590.333	111	6	6.103	0.009	1.000	123	6	0.450	0.008	46	6	0.786	0.022	Nd III + Ce II
3597.625	129	7	6.119	0.009	1.000	137	7	0.484	0.009	55	7	0.790	0.021	Nd III
3603.965	183	13	6.123	0.013	1.000	185	15	0.472	0.014	76	16	0.742	0.033	Nd III
3612.330	225	14	6.118	0.011	1.000	238	15	0.529	0.011	97	15	0.832	0.026	Nd III + La II
3621.181	75	7	6.162	0.017	1.000	68	9	0.490	0.021	40	9	0.730	0.036	Nd III + Sm II Co II, Fe II
3644.374	134	9	6.108	0.012	1.000	148	9	0.482	0.010	77	9	0.803	0.020	Nd III
HARPS														
4061.091	229	14	6.125	0.009	1.000	233	8	0.473	0.006	127	8	0.847	0.011	Nd II
4438.990	253	18	6.142	0.011	1.000	235	18	0.375	0.013	108	18	0.812	0.028	Nd II
4462.982	324	16	6.132	0.008	1.000	316	10	0.424	0.005	155	9	0.826	0.010	Nd II
4467.841	285	18	6.121	0.010	1.000	281	17	0.377	0.010	136	16	0.774	0.020	Nd II
4556.722	309	27	6.131	0.013	1.000	308	25	0.369	0.013	189	25	0.753	0.021	Nd II
4706.545	313	18	6.119	0.009	1.000	314	14	0.428	0.007	161	14	0.811	0.014	Nd II
4717.084	296	21	6.083	0.010	1.000	308	23	0.364	0.012	129	23	0.708	0.028	Nd II
4736.196	275	26	6.136	0.014	1.000	260	28	0.337	0.018	130	28	0.757	0.035	Nd II

Table 4. continued.

Wavelength	Free period					Fixed periods								Identification
						6.125 min				6.282 min				
	A	σ_A	P	σ_P	Prob.	A	σ_A	ϕ	σ_ϕ	A	σ_A	ϕ	σ_ϕ	
4763.290	347	45	6.087	0.019	1.000	341	51	0.328	0.024	173	51	0.716	0.048	Nd II
4797.139	290	18	6.125	0.010	1.000	286	16	0.380	0.009	141	16	0.777	0.018	Nd II
4799.412	290	17	6.123	0.009	1.000	283	16	0.357	0.009	124	16	0.762	0.022	Nd II
4811.342	374	21	6.126	0.008	1.000	373	17	0.404	0.007	173	17	0.795	0.016	Nd II
4818.968	336	36	6.083	0.016	1.000	360	41	0.328	0.018	159	41	0.655	0.041	Nd II
4828.566	338	27	6.126	0.012	1.000	325	29	0.353	0.014	127	29	0.775	0.037	Nd II
4947.010	291	21	6.131	0.011	1.000	280	22	0.346	0.013	116	22	0.765	0.031	Nd II
4948.996	171	16	6.126	0.014	1.000	168	17	0.328	0.016	84	17	0.726	0.032	Nd II
4959.120	351	19	6.133	0.008	1.000	345	14	0.397	0.007	168	14	0.795	0.014	Nd II
4989.932	370	18	6.139	0.008	1.000	352	12	0.368	0.006	175	12	0.785	0.011	Nd II
5033.499	310	19	6.121	0.009	1.000	313	17	0.369	0.009	139	17	0.752	0.020	Nd II
5077.143	284	18	6.129	0.010	1.000	277	19	0.329	0.011	110	19	0.739	0.028	Nd II
5089.818	279	17	6.102	0.009	1.000	289	17	0.372	0.010	117	17	0.730	0.024	Nd II
5092.790	316	18	6.130	0.009	1.000	308	15	0.383	0.008	154	15	0.786	0.016	Nd II
5096.509	274	17	6.139	0.010	1.000	261	16	0.327	0.010	129	16	0.742	0.020	Nd II
5130.586	322	17	6.135	0.008	1.000	315	11	0.418	0.006	169	10	0.816	0.010	Nd II
5132.324	341	20	6.136	0.009	1.000	332	15	0.389	0.007	180	15	0.789	0.014	Nd II
5143.324	267	19	6.122	0.011	1.000	266	19	0.347	0.012	112	19	0.741	0.027	Nd II
5176.765	280	21	6.132	0.012	1.000	283	20	0.357	0.012	148	20	0.739	0.023	Nd II
5182.597	290	17	6.110	0.009	1.000	303	16	0.346	0.009	129	16	0.707	0.020	Nd II
5212.346	309	19	6.121	0.009	1.000	311	16	0.393	0.008	152	15	0.778	0.017	Nd II
5234.198	261	14	6.125	0.008	1.000	264	9	0.384	0.006	131	9	0.764	0.012	Nd II
5255.504	363	19	6.123	0.008	1.000	363	15	0.400	0.007	158	14	0.789	0.015	Nd II
5276.861	313	17	6.112	0.008	1.000	190	6	0.423	0.006	95	6	0.816	0.012	Nd II
5356.959	332	19	6.141	0.009	1.000	321	15	0.371	0.008	132	15	0.743	0.019	Nd II
5361.158	197	20	6.115	0.015	1.000	322	16	0.359	0.008	158	16	0.763	0.017	Nd II
5361.469	267	14	6.123	0.008	1.000	269	9	0.407	0.006	133	9	0.789	0.012	Nd II
5385.884	272	20	6.120	0.011	1.000	191	23	0.327	0.019	68	23	0.746	0.055	Nd II
5399.084	381	42	6.162	0.016	1.000	279	19	0.365	0.011	147	19	0.735	0.021	Nd II
5416.363	294	26	6.112	0.013	1.000	332	48	0.285	0.023	175	48	0.740	0.044	Nd II
5431.514	304	19	6.129	0.010	1.000	307	27	0.360	0.014	153	27	0.721	0.029	Nd II
5485.692	299	19	6.130	0.010	1.000	293	19	0.376	0.011	122	19	0.794	0.026	Nd II
5533.817	276	25	6.126	0.014	1.000	255	28	0.331	0.017	115	27	0.777	0.039	Nd II
5618.984	244	32	6.137	0.020	1.000	229	35	0.350	0.024	150	35	0.759	0.038	Nd II
5702.247	296	21	6.117	0.011	1.000	304	22	0.347	0.012	129	22	0.721	0.028	Nd II
5734.535	345	36	6.150	0.015	1.000	343	35	0.343	0.016	234	35	0.722	0.024	Nd II
5804.004	286	17	6.132	0.009	1.000	279	15	0.371	0.009	133	15	0.774	0.019	Nd II
5811.564	255	17	6.112	0.010	1.000	263	16	0.357	0.010	113	16	0.723	0.024	Nd II
5825.838	296	17	6.137	0.009	1.000	280	18	0.324	0.010	108	17	0.758	0.027	Nd II
5842.358	240	16	6.140	0.010	1.000	224	16	0.357	0.012	100	16	0.791	0.027	Nd II
5865.018	235	21	6.129	0.014	1.000	227	24	0.334	0.017	67	24	0.766	0.059	Nd II
6248.259	335	43	6.170	0.019	1.000	304	45	0.337	0.024	249	45	0.738	0.029	Nd II
6341.460	266	28	6.142	0.016	1.000	255	31	0.329	0.020	112	31	0.744	0.045	Nd II
6365.524	281	32	6.105	0.017	1.000	286	36	0.329	0.020	139	35	0.704	0.041	Nd II
6637.170	321	36	6.120	0.017	1.000	335	35	0.375	0.017	238	35	0.735	0.024	Nd II
6637.942	357	27	6.137	0.012	1.000	346	26	0.357	0.012	183	26	0.761	0.023	Nd II
6650.499	340	27	6.108	0.012	1.000	355	28	0.366	0.012	168	27	0.726	0.026	Nd II
6680.125	235	39	6.129	0.025	0.999	242	46	0.300	0.031	66	46	0.667	0.112	Nd II
4445.010	274	16	6.127	0.009	1.000	274	13	0.442	0.008	133	12	0.830	0.016	Nd III + Co I
4473.290	292	15	6.124	0.008	1.000	292	9	0.456	0.005	139	9	0.843	0.011	Nd III
4514.140	247	15	6.129	0.009	1.000	247	10	0.461	0.006	143	9	0.845	0.011	Nd III
4627.260	236	13	6.120	0.008	1.000	239	9	0.426	0.007	115	9	0.808	0.014	Nd III
4651.618	308	14	6.126	0.007	1.000	306	7	0.448	0.004	141	7	0.840	0.009	Nd III
4654.312	304	15	6.125	0.008	1.000	305	8	0.475	0.004	155	8	0.859	0.009	Nd III
4689.053	308	16	6.127	0.008	1.000	303	10	0.449	0.006	151	10	0.845	0.011	Nd III
4711.331	314	15	6.120	0.007	1.000	315	9	0.458	0.005	145	9	0.842	0.011	Nd III
4759.536	227	12	6.134	0.008	1.000	223	6	0.477	0.005	126	6	0.869	0.009	Nd III
4769.622	330	35	6.183	0.016	1.000	290	9	0.461	0.005	156	9	0.861	0.010	Nd III
4788.459	312	17	6.133	0.008	1.000	305	12	0.459	0.006	160	11	0.856	0.012	Nd III
4796.499	277	14	6.128	0.008	1.000	272	8	0.469	0.005	135	8	0.865	0.010	Nd III
4821.990	287	19	6.128	0.010	1.000	289	13	0.427	0.008	158	13	0.805	0.014	Nd III
4911.651	298	14	6.128	0.007	1.000	294	8	0.472	0.004	138	8	0.867	0.010	Nd III
4912.941	330	16	6.132	0.008	1.000	323	9	0.458	0.005	159	9	0.858	0.010	Nd III
4914.090	299	15	6.126	0.008	1.000	296	9	0.491	0.005	149	9	0.883	0.010	Nd III
4927.480	254	12	6.123	0.007	1.000	257	6	0.515	0.004	125	6	0.894	0.009	Nd III
4942.638	277	14	6.130	0.008	1.000	270	8	0.450	0.005	145	8	0.849	0.010	Nd III
5050.693	247	13	6.129	0.008	1.000	240	8	0.502	0.006	121	8	0.906	0.011	Nd III
5084.656	240	18	6.126	0.012	1.000	242	16	0.458	0.011	139	16	0.839	0.019	Nd III
5084.987	297	17	6.128	0.009	1.000	298	13	0.420	0.007	151	12	0.806	0.014	Nd III
5127.047	229	12	6.124	0.008	1.000	227	8	0.538	0.006	119	8	0.927	0.011	Nd III
5151.746	240	13	6.127	0.008	1.000	238	8	0.449	0.006	125	8	0.839	0.011	Nd III
5193.031	227	11	6.121	0.008	1.000	231	7	0.520	0.005	112	7	0.897	0.011	Nd III
5203.923	217	11	6.131	0.008	1.000	213	5	0.540	0.004	113	5	0.934	0.007	Nd III
5286.724	322	16	6.125	0.008	1.000	312	13	0.399	0.007	140	13	0.809	0.015	Nd III
5294.109	254	13	6.126	0.008	1.000	253	8	0.558	0.005	125	8	0.947	0.010	Nd III
5410.094	278	15	6.117	0.008	1.000	281	10	0.496	0.006	144	10	0.875	0.012	Nd III
5429.756	161	10	6.139	0.010	1.000	155	8	0.522	0.009	89	8	0.925	0.016	Nd III + Fe I
5566.012	272	17	6.123	0.009	1.000	273	12	0.444	0.007	149	11	0.827	0.013	Nd III
5633.549	315	19	6.119	0.009	1.000	318	15	0.444	0.008	166	15	0.825	0.015	Nd III
5677.174	340	23	6.135	0.010	1.000	329	20	0.483	0.010	179	19	0.886	0.018	Nd III
5802.532	327	18	6.137	0.009	1.000	315	12	0.460	0.006	172	12	0.864	0.012	Nd III
5845.017	277	15	6.126	0.008	1.000	276	9	0.493	0.005	143	9	0.881	0.011	Nd III

Table 4. continued.

Wavelength	Free period					Fixed periods								Identification
						6.125 min				6.282 min				
	A	σ_A	P	σ_P	Prob.	A	σ_A	ϕ	σ_ϕ	A	σ_A	ϕ	σ_ϕ	
5851.529	274	14	6.122	0.008	1.000	278	8	0.458	0.005	145	8	0.837	0.009	Nd III
5987.677	317	18	6.138	0.009	1.000	306	13	0.500	0.007	164	13	0.902	0.013	Nd III
6145.062	271	14	6.132	0.008	1.000	263	9	0.506	0.006	138	9	0.908	0.011	Nd III
6327.265	266	14	6.118	0.008	1.000	271	9	0.515	0.006	141	9	0.890	0.011	Nd III
6526.638	88	8	6.110	0.015	1.000	94	9	0.450	0.016	46	9	0.795	0.033	Nd III
6550.228	325	20	6.132	0.009	1.000	291	12	0.515	0.007	151	12	0.905	0.013	Nd III
6690.821	327	24	6.133	0.011	1.000	307	26	0.412	0.014	125	26	0.851	0.034	Nd III
Sm														
UVES1														
3414.471	198	10	6.111	0.009	1.000	208	12	0.460	0.009	54	21	0.764	0.036	Sm III
3444.543	211	15	6.110	0.012	1.000	223	19	0.473	0.014	55	19	0.787	0.055	Sm III
HARPS														
4499.464	339	20	6.127	0.009	1.000	334	16	0.369	0.008	162	16	0.765	0.017	Sm II
4505.029	305	26	6.151	0.013	1.000	258	28	0.320	0.017	130	28	0.815	0.035	Sm II
4515.082	387	23	6.130	0.009	1.000	384	16	0.404	0.007	211	16	0.793	0.013	Sm II
4523.902	338	19	6.129	0.009	1.000	340	14	0.405	0.007	173	14	0.790	0.013	Sm II
4542.037	359	73	6.063	0.029	0.994	375	88	0.339	0.037	112	89	0.632	0.124	Sm II
4566.196	330	17	6.135	0.008	1.000	313	14	0.380	0.007	146	13	0.803	0.016	Sm II
4577.688	337	17	6.138	0.008	1.000	322	13	0.391	0.006	159	13	0.804	0.013	Sm II
4674.579	290	14	6.129	0.008	1.000	284	10	0.402	0.006	135	10	0.804	0.012	Sm II
4676.904	329	17	6.136	0.008	1.000	322	14	0.375	0.007	148	14	0.778	0.015	Sm II
4693.624	233	25	6.099	0.016	1.000	250	29	0.331	0.018	92	29	0.661	0.050	Sm II
4781.815	191	30	6.146	0.023	1.000	192	34	0.321	0.028	112	34	0.700	0.048	Sm II
4791.560	293	31	6.141	0.016	1.000	266	35	0.339	0.021	119	35	0.798	0.048	Sm II
4952.362	267	23	6.131	0.013	1.000	263	25	0.328	0.015	115	25	0.727	0.036	Sm II
5052.740	224	15	6.126	0.011	1.000	232	12	0.364	0.009	131	12	0.731	0.016	Sm II
5103.079	280	19	6.118	0.010	1.000	280	20	0.350	0.011	115	19	0.739	0.028	Sm II
6426.573	206	43	6.089	0.031	0.989	230	51	0.312	0.036	64	52	0.553	0.127	Sm II
6589.695	507	76	6.105	0.022	1.000	484	88	0.291	0.029	225	88	0.708	0.063	Sm II
Eu														
HARPS														
6049.502	93	22	6.127	0.036	0.891	97	26	0.276	0.044	56	26	0.641	0.075	Eu II
6173.050	136	21	6.088	0.023	1.000	141	25	0.261	0.028	41	25	0.595	0.096	Eu II
6437.636	149	14	6.093	0.015	1.000	154	16	0.271	0.017	74	16	0.628	0.035	Eu II
6645.102	175	15	6.161	0.013	1.000	149	13	0.256	0.015	101	14	0.669	0.022	Eu II
Gd														
UVES1														
3418.714	268	20	6.134	0.013	1.000	258	24	0.606	0.016	106	25	0.854	0.037	Gd II
3451.223	238	25	6.128	0.018	1.000	232	30	0.543	0.021	121	30	0.805	0.040	Gd II
3473.216	209	14	6.123	0.012	1.000	213	15	0.581	0.012	96	15	0.864	0.026	Gd II
3481.771	186	11	6.135	0.011	1.000	180	13	0.581	0.012	76	13	0.834	0.027	Gd II
3512.199	138	12	6.144	0.015	1.000	130	14	0.583	0.018	62	14	0.824	0.037	Gd II
3528.508	188	18	6.141	0.013	1.000	172	23	0.525	0.022	49	23	0.701	0.077	Gd II
3622.791	320	30	6.111	0.013	1.000	336	38	0.447	0.018	112	38	0.748	0.053	Gd II
HARPS														
4498.285	193	21	6.083	0.016	1.000	209	22	0.490	0.017	120	22	0.822	0.030	Gd II
4732.597	240	23	6.160	0.015	1.000	235	21	0.506	0.014	182	21	0.882	0.019	Gd II
5092.228	270	29	6.138	0.016	1.000	262	31	0.438	0.019	137	30	0.840	0.036	Gd II
5186.893	140	31	6.146	0.034	0.983	132	36	0.461	0.044	84	36	0.864	0.069	Gd II
5560.666	291	54	6.188	0.028	0.999	245	61	0.460	0.040	203	61	0.879	0.048	Gd II
Tb														
HARPS														
5505.391	427	26	6.140	0.009	1.000	413	16	0.940	0.006	251	16	0.338	0.010	Tb III
5847.213	416	34	6.152	0.013	1.000	405	29	0.929	0.012	277	29	0.316	0.017	Tb III
6092.916	258	23	6.133	0.013	1.000	252	23	0.952	0.015	144	22	0.349	0.026	Tb III
6323.570	340	24	6.163	0.011	1.000	304	22	0.851	0.012	190	22	0.277	0.019	Tb III
6511.043	261	34	6.125	0.019	1.000	246	39	0.881	0.025	113	38	0.309	0.055	Tb III
6537.786	275	51	6.134	0.028	0.999	261	60	0.846	0.037	107	59	0.275	0.090	Tb III
6687.701	342	59	6.125	0.026	0.999	324	70	0.902	0.035	128	70	0.335	0.088	Tb III
Dy														
UVES1														
3407.780	213	12	6.103	0.010	1.000	230	14	0.485	0.010	78	14	0.809	0.010	Dy II
3429.413	356	20	6.103	0.010	1.000	382	24	0.406	0.010	114	24	0.732	0.010	Dy II
3434.349	289	16	6.136	0.009	1.000	283	14	0.449	0.008	142	14	0.712	0.009	Dy II
3534.927	222	12	6.118	0.009	1.000	227	13	0.470	0.009	85	13	0.751	0.009	Dy II
3538.492	284	14	6.120	0.009	1.000	292	14	0.467	0.008	114	15	0.752	0.009	Dy II
3550.198	312	17	6.126	0.009	1.000	315	19	0.453	0.010	109	19	0.724	0.009	Dy II
3563.131	307	18	6.124	0.010	1.000	317	18	0.443	0.009	136	18	0.729	0.010	Dy II
3602.797	144	33	6.352	0.042	0.976	178	39	0.315	0.035	190	39	0.687	0.042	Dy II
3619.127	224	11	6.124	0.009	1.000	228	12	0.482	0.009	78	12	0.757	0.009	Dy III
3919.415	287	13	6.129	0.008	1.000	278	14	0.490	0.008	95	14	0.728	0.008	Dy III
HARPS														
4468.127	298	23	6.135	0.012	1.000	288	23	0.417	0.013	143	23	0.823	0.026	Dy II
4503.232	243	28	6.132	0.017	1.000	254	27	0.449	0.017	183	26	0.807	0.024	Dy II
4573.834	268	29	6.110	0.016	1.000	272	33	0.367	0.019	120	33	0.746	0.044	Dy II
4731.843	318	22	6.127	0.011	1.000	314	22	0.393	0.011	139	22	0.792	0.026	Dy II
4923.162	287	27	6.172	0.014	1.000	234	30	0.356	0.021	146	30	0.833	0.033	Dy II

Table 4. continued.

Wavelength	Free period					Fixed periods								Identification
						6.125 min				6.282 min				
	A	σ_A	P	σ_P	Prob.	A	σ_A	ϕ	σ_ϕ	A	σ_A	ϕ	σ_ϕ	
4409.880	367	20	6.131	0.008	1.000	355	14	0.452	0.006	183	13	0.859	0.012	Dy III
4502.903	376	27	6.135	0.011	1.000	367	22	0.432	0.010	212	22	0.828	0.017	Dy III
4572.891	325	18	6.125	0.009	1.000	326	12	0.505	0.006	171	12	0.889	0.012	Dy III
5730.329	354	25	6.119	0.011	1.000	360	21	0.464	0.010	193	21	0.839	0.018	Dy III
6655.463	289	53	6.203	0.028	0.999	254	59	0.517	0.037	249	59	0.908	0.038	Dy III 6655.375 + C I 6655.517
Ho														
UVES1														
3398.913	181	13	6.097	0.013	1.000	195	16	0.608	0.013	72	16	0.934	0.036	Ho II
3416.431	283	22	6.114	0.013	1.000	292	26	0.618	0.015	112	26	0.911	0.038	Ho II
3456.007	354	21	6.116	0.010	1.000	349	20	0.657	0.010	178	21	0.929	0.019	Ho II
3581.420	291	23	6.116	0.013	1.000	291	25	0.686	0.014	143	26	0.966	0.029	Ho III
Er														
UVES1														
3307.460	122	28	6.068	0.038	0.960	138	36	0.418	0.041	55	36	0.790	0.104	Er II
3486.795	146	13	6.119	0.016	1.000	156	16	0.476	0.017	67	16	0.781	0.038	Er II
3559.885	253	18	6.132	0.013	1.000	256	20	0.529	0.013	132	20	0.812	0.024	Er II
3633.527	224	19	6.137	0.015	1.000	220	21	0.481	0.015	127	21	0.752	0.026	Er II
HARPS														
4630.867	209	18	6.126	0.013	1.000	209	19	0.465	0.015	97	19	0.852	0.032	Er II
4675.634	187	14	6.117	0.012	1.000	191	12	0.564	0.011	114	12	0.934	0.018	Er II
5028.892	218	37	6.024	0.024	0.999	186	46	0.466	0.039	51	45	0.904	0.143	Er II
6015.724	88	20	6.055	0.038	0.938	99	26	0.266	0.041	78	26	0.603	0.053	Er II
4421.962	102	5	6.137	0.008	1.000	97	4	0.723	0.007	51	4	0.136	0.014	Er III bl.
4735.548	351	23	6.136	0.010	1.000	343	17	0.639	0.008	209	17	0.031	0.013	Er III
Tm														
UVES1														
3462.182	230	14	6.121	0.011	1.000	236	14	0.550	0.010	109	14	0.837	0.021	Tm II
Lu														
HARPS														
4785.408	83	30	2.928	0.012	0.105	52	36	0.358	0.110	31	35	0.790	0.028	Lu II
4994.141	35	12	4.860	0.033	0.133	18	15	0.310	0.132	20	14	0.949	0.118	Lu II
6199.640	80	30	7.996	0.095	0.037	62	37	0.289	0.094	18	37	0.979	0.005	Lu II
6221.844	93	29	6.212	0.047	0.496	49	34	0.502	0.112	60	34	0.232	0.093	Lu II
Th														
HARPS														
5376.120	86	30	4.145	0.024	0.097	61	32	0.416	0.084	19	31	0.834	0.106	Th III
6599.473	111	47	4.432	0.034	0.002	132	56	0.787	0.067	162	56	0.957	0.055	Th III
Unidentified lines														
UVES1														
3469.888	140	23	6.116	0.027	0.999	245	19	0.472	0.013	62	19	0.773	0.050	
3538.886	163	10	6.125	0.011	1.000	171	12	0.425	0.011	50	12	0.719	0.038	
3555.348	237	16	6.102	0.011	1.000	262	18	0.419	0.011	111	18	0.749	0.026	Nd III 3555.356
3638.758	170	14	6.095	0.014	1.000	198	16	0.328	0.013	87	16	0.697	0.030	
4211.014	173	15	6.105	0.011	1.000	193	6	0.380	0.006	76	6	0.715	0.014	Nd III 4211.003
HARPS														
4406.138	289	18	6.116	0.010	1.000	289	19	0.393	0.011	105	19	0.784	0.030	Nd III 4406.146
4499.179	110	15	6.111	0.020	1.000	113	18	0.387	0.025	32	17	0.757	0.088	
4507.522	275	15	6.131	0.008	1.000	269	13	0.392	0.008	116	12	0.797	0.018	Nd III 4507.522
4532.095	285	15	6.126	0.008	1.000	285	11	0.400	0.007	133	11	0.788	0.014	
4534.935	223	10	6.123	0.007	1.000	223	7	0.413	0.005	97	7	0.802	0.013	Nd III 4534.941
4544.236	215	14	6.105	0.010	1.000	228	14	0.333	0.010	86	14	0.678	0.027	
4546.628	257	16	6.115	0.009	1.000	268	12	0.465	0.008	135	12	0.826	0.015	
4570.637	363	18	6.128	0.008	1.000	361	11	0.453	0.005	177	11	0.842	0.010	Nd III 4570.660
4584.509	341	25	6.129	0.011	1.000	339	25	0.403	0.012	164	24	0.794	0.025	Nd III 4584.512
4603.791	257	15	6.133	0.009	1.000	250	10	0.423	0.007	135	10	0.822	0.013	
4604.590	124	10	6.123	0.012	1.000	128	9	0.363	0.012	65	9	0.735	0.024	Nd III 4604.606
4621.174	356	28	6.151	0.012	1.000	332	26	0.431	0.013	202	26	0.844	0.021	
4631.875	250	20	6.131	0.012	1.000	251	20	0.362	0.013	119	20	0.746	0.028	
4642.979	242	16	6.126	0.010	1.000	240	13	0.421	0.009	135	13	0.810	0.016	Nd III 4642.973
4650.210	273	25	6.143	0.014	1.000	247	28	0.323	0.018	102	28	0.788	0.045	
4654.039	304	15	6.125	0.008	1.000	229	8	0.455	0.006	122	8	0.860	0.012	Nd III 4654.014
4683.683	195	19	6.114	0.015	1.000	189	22	0.368	0.019	75	22	0.781	0.047	
4685.816	344	38	6.137	0.017	1.000	338	42	0.415	0.020	171	41	0.811	0.039	
4688.177	83	24	6.178	0.045	0.628	88	23	0.358	0.043	81	23	0.769	0.047	Nd III 4688.134
4688.632	104	20	6.195	0.030	0.996	61	29	0.408	0.076	32	29	0.012	0.146	Nd III 4688.690 + Tb II
4693.286	219	11	6.129	0.008	1.000	216	9	0.430	0.007	101	9	0.825	0.014	
4713.531	269	14	6.136	0.008	1.000	262	9	0.459	0.005	144	8	0.856	0.010	Nd III 4713.495
4720.752	229	16	6.150	0.011	1.000	209	16	0.415	0.013	110	16	0.850	0.024	Nd III 4720.740
4722.845	282	18	6.136	0.010	1.000	272	17	0.370	0.010	133	17	0.779	0.021	Nd III 4722.846
4723.710	253	41	6.071	0.023	0.999	280	48	0.366	0.027	122	48	0.654	0.063	
4734.757	237	25	6.144	0.016	1.000	220	27	0.443	0.020	127	26	0.865	0.034	Nd III 4734.731
4746.003	244	12	6.125	0.008	1.000	245	8	0.431	0.005	113	8	0.817	0.012	Nd III 4745.983
4748.168	29	9	6.566	0.054	0.375	17	11	0.642	0.103	11	11	0.465	0.004	
4769.314	330	35	6.183	0.016	1.000	251	40	0.309	0.026	180	40	0.803	0.036	
4770.899	150	8	6.124	0.008	1.000	152	6	0.420	0.007	70	6	0.801	0.015	Nd III 4770.884

Table 4. continued.

Wavelength	Free period					Fixed periods								Identification
						6.125 min				6.282 min				
	A	σ_A	P	σ_P	Prob.	A	σ_A	ϕ	σ_ϕ	A	σ_A	ϕ	σ_ϕ	
4787.429	184	43	6.095	0.034	0.967	222	50	0.353	0.036	138	50	0.646	0.057	
4794.247	329	19	6.117	0.009	1.000	333	15	0.409	0.007	160	14	0.787	0.015	Nd III 4794.224
4799.910	201	10	6.135	0.008	1.000	192	8	0.419	0.007	95	8	0.835	0.014	Nd III 4799.887
4804.717	245	20	6.092	0.012	1.000	255	20	0.401	0.013	134	20	0.756	0.025	Nd III 4804.719
4810.374	338	18	6.128	0.008	1.000	324	13	0.404	0.006	158	13	0.818	0.013	Nd III 4810.369
4821.110	287	19	6.128	0.010	1.000	290	16	0.414	0.009	155	16	0.794	0.017	Nd III 4821.112
4853.382	406	43	6.134	0.016	1.000	395	49	0.376	0.020	156	49	0.788	0.051	
4866.715	344	30	6.136	0.013	1.000	339	27	0.399	0.013	225	26	0.785	0.019	
4904.666	195	15	6.118	0.012	1.000	190	16	0.391	0.014	87	16	0.797	0.030	
4951.944	220	12	6.134	0.008	1.000	212	10	0.412	0.008	95	10	0.824	0.018	Nd III 4951.948
4956.202	181	13	6.143	0.011	1.000	176	11	0.388	0.011	107	11	0.781	0.018	
4972.842	153	12	6.105	0.012	1.000	159	15	0.349	0.015	43	14	0.695	0.054	
4976.801	282	20	6.094	0.011	1.000	305	23	0.370	0.012	100	23	0.680	0.037	
5012.933	324	16	6.127	0.008	1.000	324	10	0.430	0.005	154	10	0.817	0.011	
5064.040	282	18	6.118	0.010	1.000	284	15	0.416	0.009	145	15	0.799	0.017	
5078.332	212	22	6.109	0.015	1.000	223	23	0.437	0.017	110	23	0.791	0.035	
5083.846	291	21	6.105	0.011	1.000	301	21	0.410	0.011	133	21	0.772	0.026	Nd III 5083.860
5091.671	294	23	6.134	0.012	1.000	289	24	0.391	0.013	137	23	0.790	0.028	
5106.609	298	18	6.122	0.009	1.000	293	17	0.356	0.009	124	17	0.758	0.022	
5140.498	282	27	6.127	0.014	1.000	299	27	0.396	0.015	163	27	0.751	0.027	
5190.311	204	23	6.133	0.017	1.000	189	25	0.389	0.021	108	25	0.817	0.038	
5213.243	363	32	6.168	0.013	1.000	289	35	0.307	0.020	170	35	0.819	0.034	
5213.727	280	37	6.145	0.020	1.000	267	40	0.397	0.024	196	39	0.791	0.033	
5277.200	222	17	6.106	0.012	1.000	227	19	0.384	0.013	91	19	0.753	0.034	
5342.398	229	21	6.107	0.014	1.000	236	21	0.429	0.014	142	20	0.796	0.024	
5368.583	238	26	6.181	0.017	1.000	194	29	0.375	0.024	146	28	0.822	0.032	Nd III 5368.581
5373.005	398	35	6.108	0.013	1.000	404	34	0.447	0.014	226	34	0.821	0.024	
5397.851	309	23	6.116	0.011	1.000	313	22	0.402	0.011	154	21	0.781	0.023	
5432.638	202	14	6.143	0.011	1.000	186	15	0.400	0.013	90	14	0.838	0.026	
5441.654	281	25	6.154	0.014	1.000	275	22	0.428	0.013	202	21	0.809	0.018	Nd III 5441.630
5467.324	300	30	6.114	0.015	1.000	313	34	0.355	0.017	130	34	0.715	0.042	
5471.402	377	26	6.126	0.011	1.000	374	26	0.423	0.011	163	26	0.818	0.026	
5502.872	275	16	6.137	0.009	1.000	268	12	0.417	0.008	136	12	0.819	0.015	
5521.469	170	16	6.125	0.014	1.000	173	16	0.434	0.015	102	16	0.810	0.026	
5527.936	217	43	6.127	0.030	0.997	234	51	0.466	0.035	63	51	0.785	0.130	
5530.826	238	16	6.129	0.010	1.000	234	15	0.429	0.010	119	15	0.825	0.021	Nd III 5530.860
5533.381	281	32	6.108	0.017	1.000	275	37	0.282	0.021	104	37	0.690	0.057	
5536.510	341	27	6.130	0.012	1.000	339	28	0.370	0.013	165	28	0.762	0.028	
5555.726	194	46	6.231	0.037	0.955	89	55	0.317	0.098	147	54	0.845	0.060	
5556.114	395	44	6.105	0.016	1.000	403	48	0.464	0.019	205	48	0.835	0.038	
5604.916	253	34	6.145	0.025	1.000	220	40	0.316	0.029	68	40	0.879	0.094	+ Ca I 5604.939
5617.674	242	38	6.131	0.023	1.000	242	42	0.350	0.027	171	41	0.728	0.039	
5623.569	335	45	6.101	0.020	1.000	375	52	0.313	0.022	150	52	0.617	0.055	
5654.979	174	10	6.123	0.009	1.000	178	7	0.422	0.007	88	7	0.797	0.014	Nd III 5654.965
5673.185	302	37	6.117	0.018	1.000	312	41	0.420	0.021	160	41	0.788	0.042	
5680.682	339	39	6.136	0.017	1.000	367	39	0.406	0.017	234	39	0.751	0.027	
5705.229	263	20	6.133	0.011	1.000	254	18	0.409	0.011	146	17	0.811	0.020	Nd III 5705.238
5713.777	194	36	6.173	0.028	0.999	173	41	0.414	0.038	136	40	0.823	0.048	
5714.329	265	35	6.104	0.019	1.000	271	39	0.366	0.023	136	39	0.735	0.047	Nd III 5714.366
5796.994	287	28	6.121	0.015	1.000	291	30	0.412	0.017	142	30	0.790	0.034	
5852.421	253	14	6.142	0.009	1.000	238	12	0.398	0.008	121	12	0.820	0.017	
5920.707	306	25	6.140	0.012	1.000	287	26	0.401	0.014	141	25	0.828	0.030	
5926.403	253	25	6.103	0.015	1.000	272	27	0.408	0.016	128	27	0.747	0.034	
5960.612	277	23	6.131	0.013	1.000	275	25	0.381	0.015	114	24	0.778	0.035	
5993.170	266	46	6.135	0.026	0.999	270	52	0.392	0.031	174	51	0.767	0.048	
5998.263	257	31	6.137	0.018	1.000	237	35	0.397	0.024	120	35	0.834	0.047	
6012.286	340	21	6.116	0.009	1.000	351	18	0.397	0.008	163	17	0.763	0.018	
6014.550	327	20	6.123	0.009	1.000	333	15	0.431	0.007	174	15	0.806	0.014	
6023.314	174	40	6.137	0.034	0.974	156	47	0.287	0.049	51	47	0.796	0.149	
6038.492	278	26	6.103	0.014	1.000	299	29	0.384	0.016	104	29	0.708	0.045	
6044.651	264	24	6.110	0.014	1.000	269	26	0.374	0.016	115	26	0.747	0.037	
6093.852	295	21	6.116	0.011	1.000	301	22	0.401	0.012	131	21	0.776	0.027	
6105.792	272	28	6.117	0.016	1.000	276	29	0.392	0.017	163	29	0.767	0.029	
6148.852	220	17	6.139	0.012	1.000	214	16	0.430	0.012	112	16	0.830	0.024	
6172.552	217	25	6.133	0.018	1.000	219	29	0.320	0.021	103	28	0.702	0.045	
6193.598	190	38	6.197	0.031	0.995	140	45	0.361	0.051	116	45	0.837	0.063	
6201.765	260	43	6.097	0.024	0.999	293	51	0.286	0.028	103	51	0.568	0.078	
6206.097	214	39	6.031	0.026	0.999	240	45	0.394	0.030	169	45	0.679	0.042	
6251.136	321	28	6.140	0.013	1.000	300	31	0.373	0.017	138	31	0.806	0.037	
6254.676	231	19	6.134	0.012	1.000	215	21	0.364	0.016	89	20	0.810	0.038	
6273.707	271	23	6.121	0.013	1.000	280	22	0.422	0.013	156	22	0.790	0.023	Nd III 6273.673
6286.059	172	48	6.025	0.040	0.718	194	57	0.291	0.047	138	58	0.567	0.065	
6328.438	152	25	6.131	0.025	0.999	151	30	0.352	0.032	69	29	0.745	0.069	
6351.919	154	17	6.070	0.017	0.743	163	51	0.299	0.050	87	52	0.632	0.093	
6417.128	242	14	6.118	0.009	1.000	239	11	0.416	0.008	114	11	0.810	0.016	
6434.946	221	41	6.104	0.028	0.998	237	49	0.293	0.033	80	49	0.621	0.097	
6524.464	353	27	6.127	0.012	1.000	348	26	0.412	0.012	175	26	0.809	0.024	
6579.551	273	47	6.121	0.026	0.999	273	54	0.383	0.032	143	53	0.770	0.061	
6667.494	226	62	6.097	0.040	0.714	286	73	0.344	0.040	166	73	0.612	0.069	

Table 5. Comparison of the pulsational amplitudes and phases near the magnetic maximum at different years calculated with the main pulsation period P = 6.125 min in 2001 and 2004, and P = 6.20 min in 2003.

WL Å	2001 phase = 0.872				2003 phase = 0.083				2004 phase = 0.867				2004 phase = 0.944				
	A	σ_A	ϕ	σ_ϕ	A	σ_A	ϕ	σ_ϕ	A	σ_A	ϕ	σ_ϕ	A	σ_A	ϕ	σ_ϕ	
5284.690					319	37	0.678	0.017	338	11	0.685	0.006	259	11	0.642	0.007	Pr III
5299.986					291	31	0.702	0.016	327	12	0.678	0.006	246	10	0.641	0.007	Pr III
5844.406					301	38	0.571	0.020	305	14	0.603	0.008	299	15	0.576	0.008	Pr III
5998.935					254	30	0.571	0.019	382	18	0.606	0.008	329	15	0.587	0.008	Pr III
6160.238					195	19	0.610	0.016	342	12	0.657	0.006	251	10	0.624	0.006	Pr III
6692.225	315	41	0.519	0.021					245	61	0.547	0.040	317	27	0.501	0.014	Pr III
6706.708	307	17	0.594	0.009	294	65	0.497	0.037	371	27	0.601	0.012	359	15	0.569	0.007	Pr III
4959.120					224	30	0.381	0.023	345	14	0.397	0.007	254	9	0.383	0.006	Nd II
5182.597					197	34	0.331	0.028	303	16	0.346	0.009	251	11	0.336	0.007	Nd II
5319.81					234	36	0.394	0.027					262	9	0.398	0.005	Nd II
6637.942	264	16	0.348	0.010					346	26	0.357	0.012	244	13	0.346	0.009	Nd II
6650.499	286	21	0.348	0.012					355	28	0.366	0.012	241	12	0.358	0.008	Nd II
6680.125					199	90	0.251	0.069	242	46	0.300	0.031	157	19	0.327	0.019	Nd II
5286.724					250	31	0.353	0.021	312	13	0.399	0.007	267	9	0.381	0.006	Nd III
5294.109					180	23	0.520	0.022	253	8	0.558	0.005	188	8	0.540	0.007	Nd III
5566.012					182	23	0.430	0.022	273	12	0.444	0.007	198	7	0.400	0.006	Nd III
5677.174					229	34	0.458	0.025	329	20	0.483	0.010	236	9	0.431	0.006	Nd III
5845.017					239	27	0.464	0.019	276	9	0.493	0.005	227	8	0.466	0.006	Nd III
5851.529					292	34	0.447	0.020	278	8	0.458	0.005	261	9	0.431	0.006	Nd III
5987.677					264	26	0.480	0.017	306	13	0.500	0.007	245	8	0.464	0.006	Nd III
6145.062					232	28	0.472	0.021	263	9	0.506	0.006	194	9	0.482	0.008	Nd III
6690.821	311	14	0.415	0.007	221	51	0.412	0.039	307	26	0.412	0.014	235	11	0.399	0.008	Nd III
6173.050					213	58	0.331	0.041	141	25	0.261	0.028	79	10	0.248	0.021	Eu II
6645.102	142	8	0.232	0.010					149	13	0.256	0.015	110	8	0.252	0.012	Eu II
5847.213					394	63	0.914	0.027	405	29	0.929	0.012	359	23	0.869	0.010	Tb III
6511.043					223	76	0.846	0.056	246	39	0.881	0.025	329	23	0.824	0.011	Tb III
6687.701	296	34	0.869	0.018					324	70	0.902	0.035	197	23	0.846	0.018	Tb III

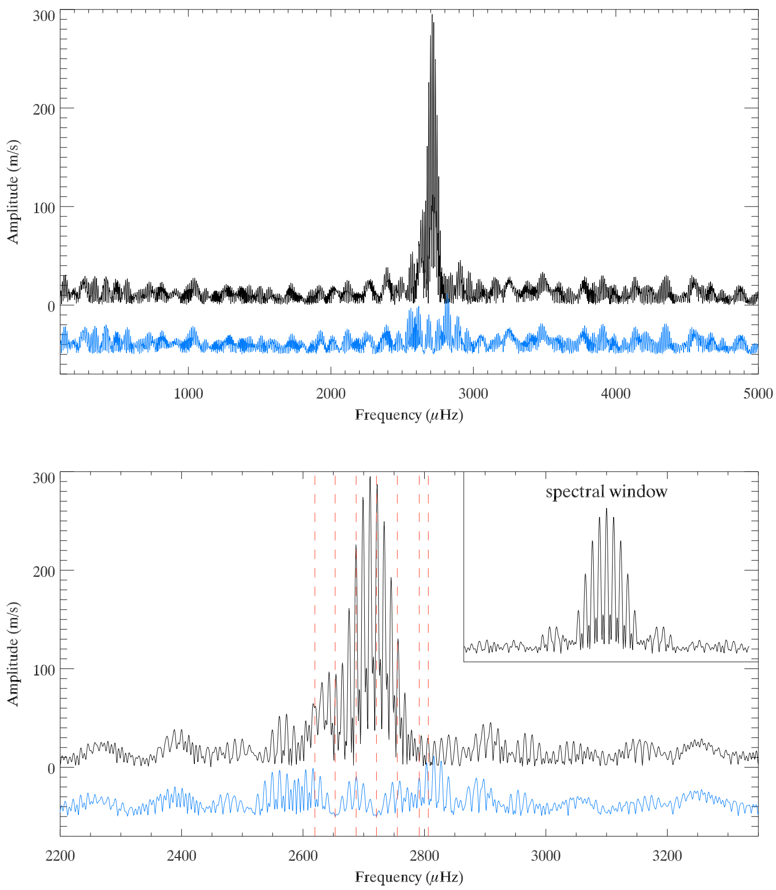

Fig. 9. Amplitude spectra of Nd III spectral lines observed in 2001. In each panel the upper curve shows the original amplitude spectrum, whereas the lower curve (shifted downwards for better visibility) represents the Fourier transform of the RV-values after prewhitening with the two main RV frequencies of 2720.96 and 2652.96 μHz, which account for most of the RV power in the data set. The lower panel represents an enlarged view of the upper one. The spectral window of the data set is inserted. The vertical dashed lines indicate photometric frequencies according to Kurtz et al. (2005).